Article

Current Biology

Movements during sleep reveal the developmental emergence of a cerebellar-dependent internal model in motor thalamus

Graphical abstract

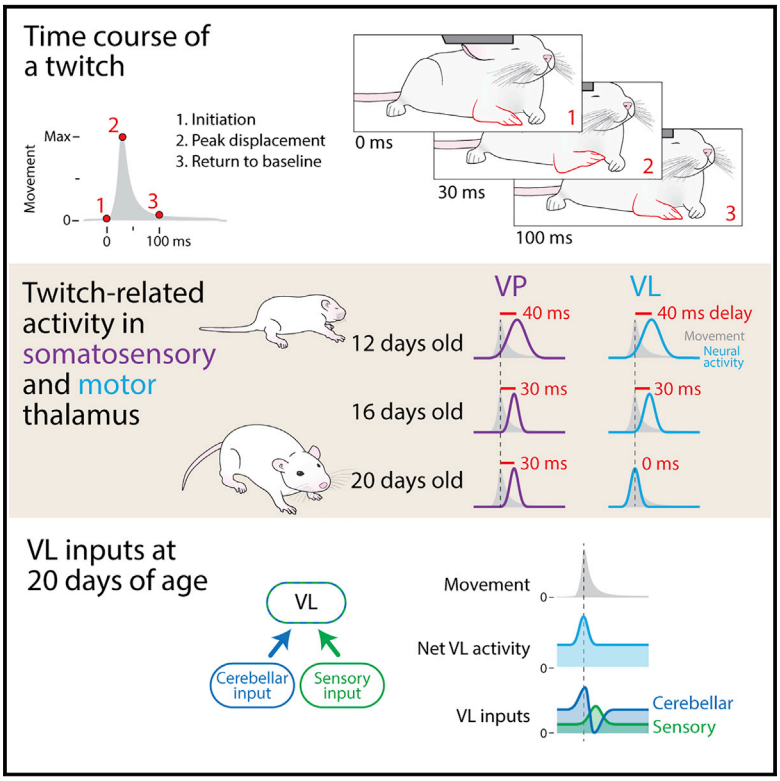

Highlights

- Twitches trigger activity in thalamus and cortex beyond the early postnatal period
- Twitch-related activity is spatiotemporally refined by the 3rd postnatal week
- Motor thalamus activity reflects an internal model of a twitch
- This internal model of movement depends on cerebellar output

Authors

James C. Dooley, Greta Sokoloff, Mark S. Blumberg

Correspondence

james-c-dooley@uiowa.edu

In brief

Internal models of movement enable the production of coordinated behavior; however, we do not know when internal models first develop. Using myoclonic twitches, movements that are produced exclusively during sleep, Dooley et al. establish the emergence of a cerebellar-dependent internal model of movement in motor thalamus of rats at 20 days of age.

Dooley et al., 2021, Current Biology *31*, 1–11
December 20, 2021
https://doi.org/10.1016/j.cub.2021.10.014

CellPress

Current Biology

CellPress
OPEN ACCESS

Article

Movements during sleep reveal the developmental emergence of a cerebellar-dependent internal model in motor thalamus

James C. Dooley,[1,4,*] Greta Sokoloff,[1,3] and Mark S. Blumberg[1,2,3]
[1]Department of Psychological & Brain Sciences, University of Iowa, Iowa City, IA 52242, USA
[2]Interdisciplinary Graduate Program in Neuroscience, University of Iowa, Iowa City, IA 52245, USA
[3]Iowa Neuroscience Institute, University of Iowa, Iowa City, IA 52242, USA
[4]Lead contact
*Correspondence: james-c-dooley@uiowa.edu
https://doi.org/10.1016/j.cub.2021.10.014

SUMMARY

With our eyes closed, we can track a limb's moment-to-moment location in space. If this capacity relied solely on sensory feedback from the limb, we would always be a step behind because sensory feedback takes time: for the execution of rapid and precise movements, such lags are not tolerable. Nervous systems solve this problem by computing representations—or internal models—that mimic movements as they are happening, with the associated neural activity occurring after the motor command but before sensory feedback. Research in adults indicates that the cerebellum is necessary to compute internal models. What is not known, however, is when—and under what conditions—this computational capacity develops. Here, taking advantage of the unique kinematic features of the discrete, spontaneous limb twitches that characterize active sleep, we captured the developmental emergence of a cerebellar-dependent internal model. Using rats at postnatal days (P) 12, P16, and P20, we compared neural activity in the ventral posterior (VP) and ventral lateral (VL) thalamic nuclei, both of which receive somatosensory input but only the latter of which receives cerebellar input. At all ages, twitch-related activity in VP lagged behind the movement, consistent with sensory processing; similar activity was observed in VL through P16. At P20, however, VL activity no longer lagged behind movement but instead precisely mimicked the movement itself; this activity depended on cerebellar input. In addition to demonstrating the emergence of internal models of movement, these findings implicate twitches in their development and calibration through, at least, the preweanling period.

INTRODUCTION

Many functional behaviors demand the production of precisely timed movements. Proper execution of these movements requires that motor commands are coordinated with movement-related sensory feedback (or reafference).[1–3] This coordination is made possible by the production of copies of motor commands (or corollary discharges) that contribute to the computation of an internal model in the cerebellum and other structures, providing the animal with an accurate, moment-to-moment representation of its own movements.[4–7] One of the major targets of the cerebellum is the motor thalamus—the ventral lateral nucleus (VL)—which projects to primary motor cortex (M1).[8–13] In its entirety, this system enables flexible and adaptive updating of movements in real time.

To understand how internal representations of movement contribute to behavior, researchers have assessed learning-related changes in cerebellar activity as an animal learns a novel behavioral task[14–16] or the behavioral consequences of manipulating the cerebellothalamic system.[9,13,17] Although these experimental approaches have effectively revealed cerebellar functioning in adults, they are not suitable for determining when internal representations first develop. Here, we address this developmental question by exploiting the spontaneous limb movements that are performed abundantly throughout early development during active (or REM) sleep, known as myoclonic twitches.

In infant rats, the movements of the limbs and whiskers during sleep exhibit several features that make them well-suited for assessing sensorimotor development.[18,19] Specifically, twitches are brief and discrete, hundreds of thousands of them are produced each day, and they reliably trigger reafferent activity throughout the sensorimotor system.[19] In addition, the motor commands that trigger these movements also produce a corollary discharge that is conveyed to the cerebellum via precerebellar nuclei.[20] These features of twitches suggest that they are uniquely able to provide the precise information about the timing of expected and actual sensory feedback upon which the computation of an internal model depends. Moreover, given that the cerebellar system is still undergoing substantial anatomical and functional development between postnatal day (P) 12 and P20,[21–25] a role for twitches in the development of internal

Please cite this article in press as: Dooley et al., Movements during sleep reveal the developmental emergence of a cerebellar-dependent internal model in motor thalamus, Current Biology (2021), https://doi.org/10.1016/j.cub.2021.10.014

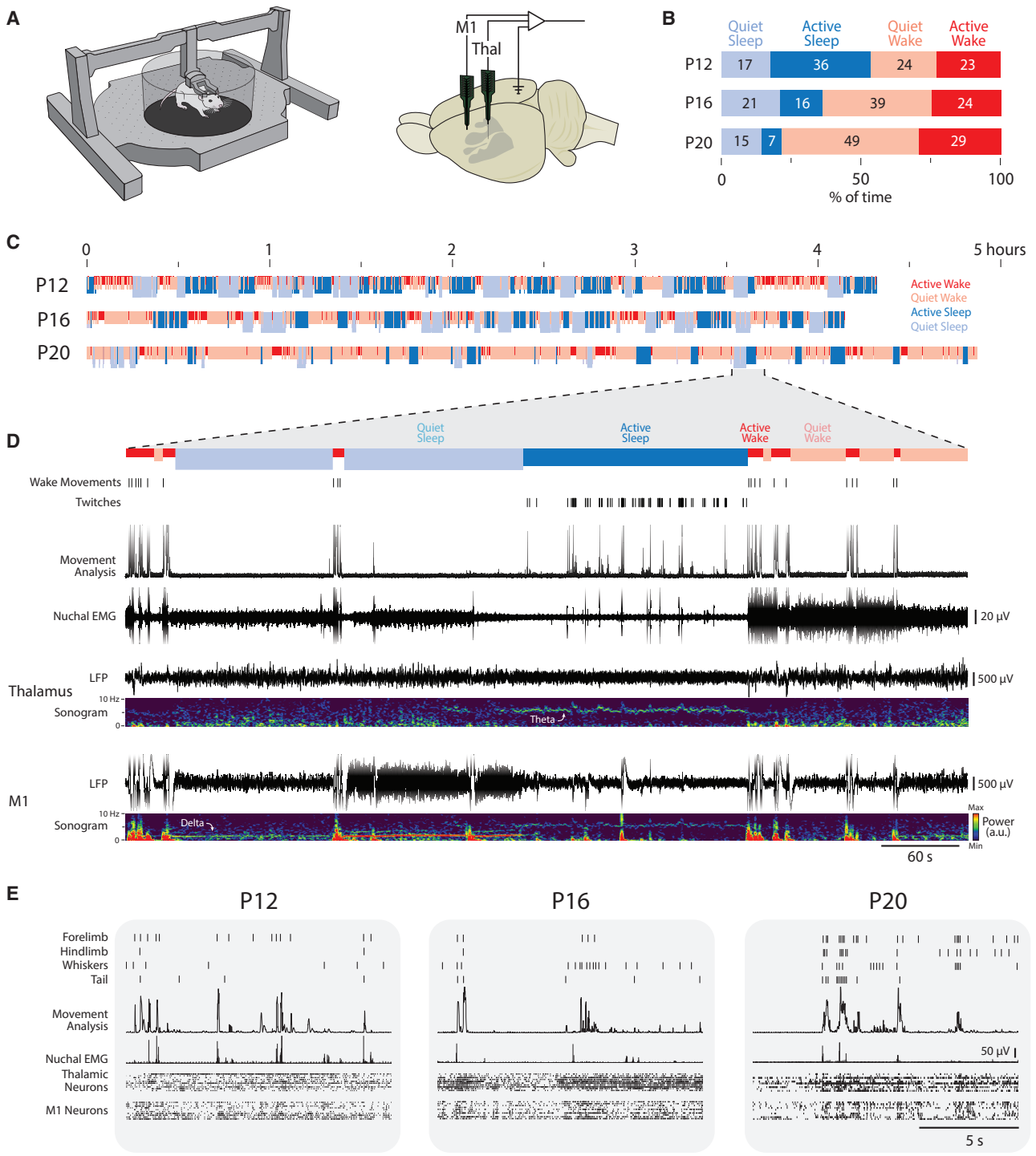

Figure 1. Infant rats reliably sleep and twitch in the Mobile HomeCage

(A) Left: an illustration of the Mobile HomeCage used to collect behavioral and electrophysiological data across sleep and wake from head-fixed rats. Right: an infant rat brain, with primary somatosensory cortex denoted in gray, shows the relative insertion points of the recording sites in M1 and thalamus and the location of the reference and ground in contralateral occipital cortex.

(B) Mean percentage of time spent in quiet sleep (light blue), active sleep (dark blue), quiet wake (light red), and active wake (dark red) at P12, P16, and P20. Numbers indicate the percentage of time for each category.

(C) Representative sleep staging throughout the recording session for a rat at each age. Periods of active wake (dark red), quiet wake (light red), active sleep (dark blue), and quiet sleep (light blue) are shown.

(legend continued on next page)

Please cite this article in press as: Dooley et al., Movements during sleep reveal the developmental emergence of a cerebellar-dependent internal model in motor thalamus, Current Biology (2021), https://doi.org/10.1016/j.cub.2021.10.014

models would require that they continue to drive neural activity in the sensorimotor system at ages beyond those that we have previously investigated.

Here, using P12, P16, and P20 rats, we examined movement-related activity in VL and M1, as well as the thalamic ventral posterior nucleus (VP). First, we demonstrate that twitches, from P12 to P20, continue to drive topographically precise neural activity in all three structures. Next, we show that VP and VL exhibit temporal sharpening of movement-related activity such that, by P20, the duration of the neural activity closely matches the duration of the movement. Moreover, whereas movement-related activity in VP reliably lags movement at all three ages—as expected of a sensory nucleus—we find no such lag in VL activity at P20. In fact, at P20, VL activity precisely mimics the movement itself. Given that VL receives strong, direct projections from the deep cerebellar nuclei (DCN), we pharmacologically inactivated the DCN at P20 and demonstrate that the precise co-occurrence of VL activity and movement is disrupted. Altogether, these results demonstrate that, by P20, movement-related activity in VL reflects the emergence of a cerebellar-dependent capacity to accurately predict the sensory consequences of movement.

RESULTS

Movements during sleep continue to drive thalamocortical activity

To establish that movements during active sleep continue to drive thalamocortical activity beyond early infancy, we recorded neural activity in head-fixed, unanesthetized rats at P12, P16, and P20. Rats were tested in the Mobile HomeCage, which allows animals to locomote while head-fixed (Figure 1A, left). Extracellular activity was recorded in the forelimb region of M1 (P12: N = 11 pups, 121 neurons; P16: N = 12 pups, 177 neurons; P20: N = 22 pups, 259 neurons), VP (P12: N = 6 pups, 116 neurons; P16: N = 6 pups, 82 neurons; P20: N = 5 pups, 75 neurons), and VL (P12: N = 5 pups, 57 neurons; P16: N = 5 pups, 89 neurons; P20: N = 6 pups, 89 neurons; Figures 1A, right, and S1A). Neural activity, electromyographic (EMG) activity in the nuchal and biceps muscles, and high-speed video (100 frames/s) were recorded continuously for 3–6 h. Recordings were performed during the lights-on period between 1000 and 1700 hours.

Rats cycled between sleep and wake at all three ages, and as expected,[26–28] the percentage of time spent in active sleep decreased across age (Figures 1B and 1C). As seen in 10 min of representative data in a P20 rat, quiet sleep was accompanied by increased delta power in M1, whereas active sleep was accompanied by twitching, low nuchal muscle tone, and high theta power in thalamus and M1 (Figure 1D). Wake consisted of high muscle tone as well as periods of movement (active wake) interspersed with periods of quiescence (quiet wake). Representative behavioral and neurophysiological data during 15-s periods of active sleep at P12, P16, and P20 are presented in Figure 1E. Along with a significant age-related decrease in total time in active sleep during each recording session (Figure S1B), older pups also showed significantly fewer twitches (Figure S1C).

Despite the reduced rate of twitching in older pups, neurons remained responsive to twitches at all ages tested. At P12, P16, and P20, neurons in M1 increased their activity only after a movement (Figure 2A, black), similar to previous findings through P12 and consistent with the view that M1 is not involved in motor control at these ages.[29–31] Movement-responsive neurons in M1 were found during both sleep and wake (Figure 2A, gray). Although such responses are presumed to arise from thalamus, the thalamic source of sensory inputs to M1, particularly in early development, remains unclear.[32] As with M1, neurons in VP and VL also showed increased activity in response to movements produced during sleep and wake at all three ages (Figures 2B and 2C). At P12 and P16, neurons in VP exhibited either a fast response to movement (with a rapid return to baseline), a slow response (with neural activity elevated for more than 2 s), or a fast-and-slow response comprising two distinct peaks in activity (Figure S2A). However, by P20, the slow response disappeared, leaving only neurons with the fast response (Figure S2B). The existence of a slow response in VP is reminiscent of similarly transient long-duration responses to brief light flashes in the visual system, which result from cortical feedback to thalamus.[33,34] In contrast, all VL neurons exhibited a fast response regardless of age (Figures S2C and S2D). The absence of slow responses in VL suggests a difference from VP in its development of corticothalamic feedback.

Somatotopic and temporal refinement of movement-related thalamic activity

Having demonstrated that neurons in VP and VL exhibit movement-related activity through P20, we next assessed whether this activity is somatotopically and temporally precise. With respect to somatotopy, we tracked four body parts (forelimb, hindlimb, whiskers, and tail; Figures S3A and S3B) and characterized neural responses in VP and VL to movements of each part. This somatotopic analysis was necessarily restricted to twitches because wake movements typically involved simultaneous movements of multiple body parts. Neurons in both structures responded with somatotopic precision across all three ages: when a neuron was responsive to movements of one body part (e.g., forelimb), it did not respond to movements of other body parts (e.g., hindlimb, whiskers, or tail; Figures 3A and 3B; see also Figure S3C).

To assess the temporal precision of thalamic activity, we first characterized the kinematics of twitches at each age. Twitches are rapid movements, with maximum durations of <100 ms (or fewer than 10 frames; Figure S3A). Generally, these movements are characterized by rapid acceleration to a peak displacement, followed by a slow return to baseline (Figure 3C). This general

(D) Representative 600-s recording period from a P20 rat in (C). From top: wake movements, twitches, movement of any kind in each video frame, nuchal EMG, thalamic LFP and associated sonogram, and M1 LFP and associated sonogram are shown.
(E) Representative 15-s behavioral and electrophysiological records at P12, P16, and P20. From top: twitches of four different body parts, the amount of movement detected in each video frame, rectified nuchal EMG, and thalamic and M1 neural activity (each row is a different neuron) are shown.
See also Figure S1.

Please cite this article in press as: Dooley et al., Movements during sleep reveal the developmental emergence of a cerebellar-dependent internal model in motor thalamus, Current Biology (2021), https://doi.org/10.1016/j.cub.2021.10.014

Figure 2. Twitch-related reafference continues to trigger thalamocortical activity through P20

(A) Top: raster sweeps for representative twitch-responsive M1 neurons at P12, P16, and P20, with each row triggered on a different twitch. Bottom: perievent histograms (bin size = 10 ms) show the neuron's firing rate above baseline triggered on twitches (dark lines) and wake movements (light lines).

(B) Same as in (A), except for VP.

(C) Same as in (A), except for VL.

See also Figure S2.

shape was consistent across body parts and ages, with peak displacement occurring 30 ms (or three frames) after the movement was triggered (Figure S3D, right). In contrast, movements during wake exhibited more variability in peak displacement and were over ten times longer in duration (Figure S3D, left). To estimate the duration of each movement, we determined the width at half-height of the displacement curves for all body parts. There was no significant age-related change in mean movement duration ($H_{(2,143)} = 0.82$; $p = 0.66$). These results are not specific to half-height, as we found similar results using three-quarter height (Figure S3E).

We also used width at half-height to compare the duration of the neural responses to movement in VP and VL. To ensure we were making a comparison across similar populations of neurons, we restricted this analysis to the "fast" VP neurons (see Figure S2A). In VP, there was a significant effect of age on response duration ($H_{(2,55)} = 16.3$; $p < 0.001$), with durations at P12 being longer than those at P16 and P20 (Figures 3E and 3F). Furthermore, by comparing the duration of the VP response with the duration of movement, we found a significant difference at P12 ($Z_{31} = 4.43$; $p < 0.001$), but not at P16 or P20 (P16: $Z_{17} = -0.57$, $p = 0.57$; P20: $Z_{10} = 0.31$, $p = 0.79$). Thus, by P16, the increase in neural activity in VP accurately represents the temporal duration of movement.

Parallel analyses in VL also revealed a significant effect of age on response duration, with durations decreasing with age (Figure 3G; $H_{(2,63)} = 18.2$; $p < 0.001$). Unlike VP, in VL, we saw a continuous decrease in response duration at all three ages, with neural responses at P12 and P16, but not P20, exhibiting durations that were significantly longer than those of twitches (Figure 3H; P12: $Z_{24} = 4.20$, $p < 0.001$; P16: $Z_{23} = 3.36$, $p < 0.001$; P20: $Z_{22} = 1.81$, $p = 0.07$). Again, these results in VP and VL were not specific to width at half-height, as the same basic results held at three-quarter height (Figure S3E).

Divergent representations of movement in VP and VL

As demonstrated thus far, by P20, movement-related neural activity in VP and VL is somatotopically precise and matches the duration of movement. Next, we examined the difference in the timing of the peak neural responses in relation to peak displacement. We then classified movement-related neural activity as follows: activity that reliably preceded movement was classified as "motor" (Figure 4A, red); neural activity that reliably followed movement was classified as "sensory" (Figure 4A, green); and

Please cite this article in press as: Dooley et al., Movements during sleep reveal the developmental emergence of a cerebellar-dependent internal model in motor thalamus, Current Biology (2021), https://doi.org/10.1016/j.cub.2021.10.014

CellPress
OPEN ACCESS

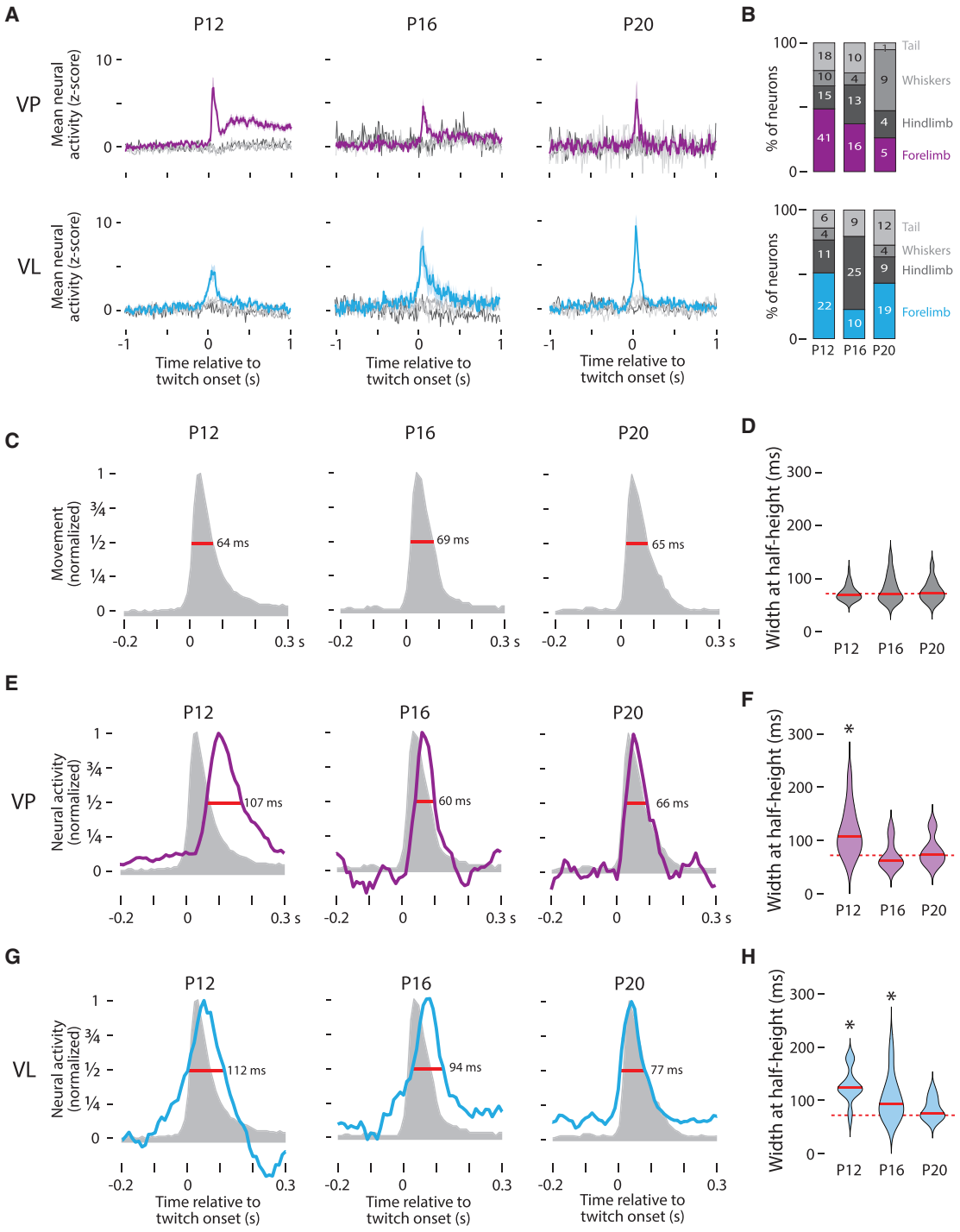

Figure 3. Twitch-related thalamic activity is spatiotemporally refined across age

(A) Mean (±SE) *Z*-scored neural activity of forelimb twitch-responsive neurons in VP (top) and VL (bottom) in response to twitches of the forelimb (purple or cyan, respectively), hindlimb (dark gray), whiskers (gray), or tail (light gray).

(B) Percentage of twitch-responsive neurons that respond to twitches of different body parts in VP (top) and VL (bottom). The number of neurons for each category is also shown.

(C) Representative normalized movement profiles for forelimb twitches at P12, P16, and P20. The widths at half-height (red lines) are also shown.

(D) Violin plots of the width at half-height for twitch displacement at each age. The solid red line is the median value at each age, and the dotted red line is the grand median across all ages.

(E) Representative twitch-related responses of VP neurons at P12, P16, and P20 (blue). The movement profiles from (C) are shown for comparison. The widths at half-height (red lines) are also shown.

(legend continued on next page)

Please cite this article in press as: Dooley et al., Movements during sleep reveal the developmental emergence of a cerebellar-dependent internal model in motor thalamus, Current Biology (2021), https://doi.org/10.1016/j.cub.2021.10.014

neural activity that reliably co-occurred with movement was classified as "internal model" (Figure 4A, blue).[16]

VP's role in transmitting somatosensory information to cortex is well established.[35] Consequently, we expected activity in VP to reflect sensory feedback, and this was exactly what we saw. We categorized over 80% of VP neurons as sensory at all three ages, with no significant change in group identity across age (Figure 4B; $\chi^2 = 5.87$; N = 146; p = 0.21; see also Figure S4A). Further, at all ages, movement-related activity in VP significantly lagged peak displacement by 30–40 ms (Figure 4C; P12: $Z_{73} = 6.69$, $p < 0.001$; P16: $Z_{38} = 4.09$, $p < 0.001$; P20: $Z_{16} = 3.16$, $p < 0.01$), consistent with the conduction delay of reafference found in other somatosensory structures.[31]

In adults, although VL does receive sensory input,[36,37] it is not strictly sensory like VP. For example, VL neurons can selectively respond to movements that are self- or other-generated,[38,39] with the activity of neurons responsive to self-generated movements being too fast to be sensory.[14,16] Other studies suggest that VL can influence the production of movement via its projections to M1.[9,13] Here, at P12 and P16, most VL neurons were classified as sensory (Figure 4B) because of a significant 30- to 40-ms lag in peak neural activity in relation to peak displacement (Figure 4C; P12: $Z_{38} = 5.12$, $p < 0.001$; P16: $Z_{39} = 4.68$, $p < 0.001$). By P20, however, most VL neurons did not exhibit a lag (Figure 4B, right; $\chi^2 = 24.7$, N = 131, $p < 0.001$; Figure 4C, right; $Z_{35} = 0.676$, p = 0.500).

Until now, we recorded VP and VL activity separately in different animals. Thus, to increase our confidence in the differential timing of twitch-related activity in VP and VL, we performed simultaneous recordings in the two nuclei in an additional set of P20 rats (n = 3; Figure 4D). Focusing on neurons that responded to forelimb movements, we again found that VP activity lagged peak limb displacement by 20 ms, with VL activity exhibiting no lag at all (Figures 4E and 4F). Given that the sensory input to VP arrives directly from the dorsal column nuclei,[40,41] the fact that movement-related activity occurred in VL 20 ms before that in VP indicates that the VL activity is unlikely to be due to reafference.

Disrupting cerebellar output at P20 unmasks sensory responses in VL

If movement-related VL activity at P20 reflects the emergence of an internal model, we would expect the cerebellum to be the source of this activity for several reasons. First, the deep cerebellar nuclei (DCN) are the dominant source of excitatory input to VL,[10] and second, the cerebellum is responsible for the precise timing of movement-related activity in VL.[16,17] Accordingly, we predicted that inactivation of the DCN at P20 would disrupt the precise timing of VL activity, resulting in activity that resembles sensory responses in VP. To test this prediction, we recorded activity in VL after injecting 0.5 μL of muscimol (N = 6 pups; 96 VL neurons) or saline (N = 6 pups; 93 VL neurons) into the DCN (Figure 5A). We targeted the interposed nucleus because (1), as part of the intermediate cerebellum, it processes proprioceptive input;[42] (2) it exhibits twitch-related activity in P8 and P12 rats;[43] and (3) together with the dentate nucleus, the interposed nucleus projects to VL (Figures S5A and S5B).[44] DCN inactivation had no effect on the percentage of time spent in active sleep (Figure S5C), though it did cause a small but significant decrease in VL activity (Figure S5D; $F_{(1,152)} = 8.42$; $p < 0.005$). DCN inactivation also had no effect on the rate of twitching (Figure S5E), the somatotopic distribution of twitch-responsive neurons (Figure S5F), or the kinematics of movements during sleep (Figure S5G). There were also no significant group differences in the duration (width at half-height) of twitches or VL activity (Figure S5H).

As predicted, DCN inactivation with muscimol shifted the peak of movement-related activity in VL (Figures 5B, S5I, and S5J), resulting in activity in VL that resembled the sensory responses in VP (Figure S4A). Whereas most neurons in the saline group showed peak activity consistent with the action of an internal model, the majority of neurons in the muscimol group showed peak activity consistent with sensory processing, a statistically significant shift (Figure 5C; $\chi^2 = 11.9$; N = 95; $p < 0.005$). Altogether, whereas movement-related activity in VL neurons of muscimol-injected pups exhibited a significant 20-ms lag in peak displacement (Figure 5D; $Z_{39} = 4.04$; $p < 0.001$), no such lag occurred in the saline-injected pups ($Z_{56} = -0.11$; p = 0.91).

DISCUSSION

We demonstrate here that movements during active sleep continue to trigger somatotopically precise neural activity in VP, VL, and M1 beyond the early postnatal period. We also show that movement-related activity in VP and VL is refined during postnatal development such that, by P20, the response duration is as brief as the movement itself. Moreover, whereas the neural response in VP reliably lags movement by 20–30 ms, indicative of reafference, the response in VL undergoes a developmental shift—from a reafferent response at P12 and P16 to a response at P20 that closely mimics the time course of the movement. This last finding reveals the emergence in VL of an internal model of movement that is cerebellar dependent, as inactivating the DCN disrupted this precise correspondence between VL activity and twitches. Further, DCN inactivation unmasked a reafferent response that resembled movement-related activity in VP. Given that internal models are necessary for distinguishing self-generated from other-generated sensory input, our findings help to identify the developmental emergence of the self-other distinction.

Neural representations of movement are inherently noisy.[7] Thus, to extract a signal that accurately characterizes how movements are represented in the brain, experimenters have

(F) Violin plots of the width at half-height for twitch-responsive VP neurons at each age; the solid red lines are the median value at each age. Asterisks indicate significant difference ($p < 0.0167$) between the median value for the neural response and the grand median duration of the twitch (dotted red line).
(G) Same as in (E), except for VL.
(H) Same as in (F), except for VL.
See also Figure S3.

Please cite this article in press as: Dooley et al., Movements during sleep reveal the developmental emergence of a cerebellar-dependent internal model in motor thalamus, Current Biology (2021), https://doi.org/10.1016/j.cub.2021.10.014

CellPress
OPEN ACCESS

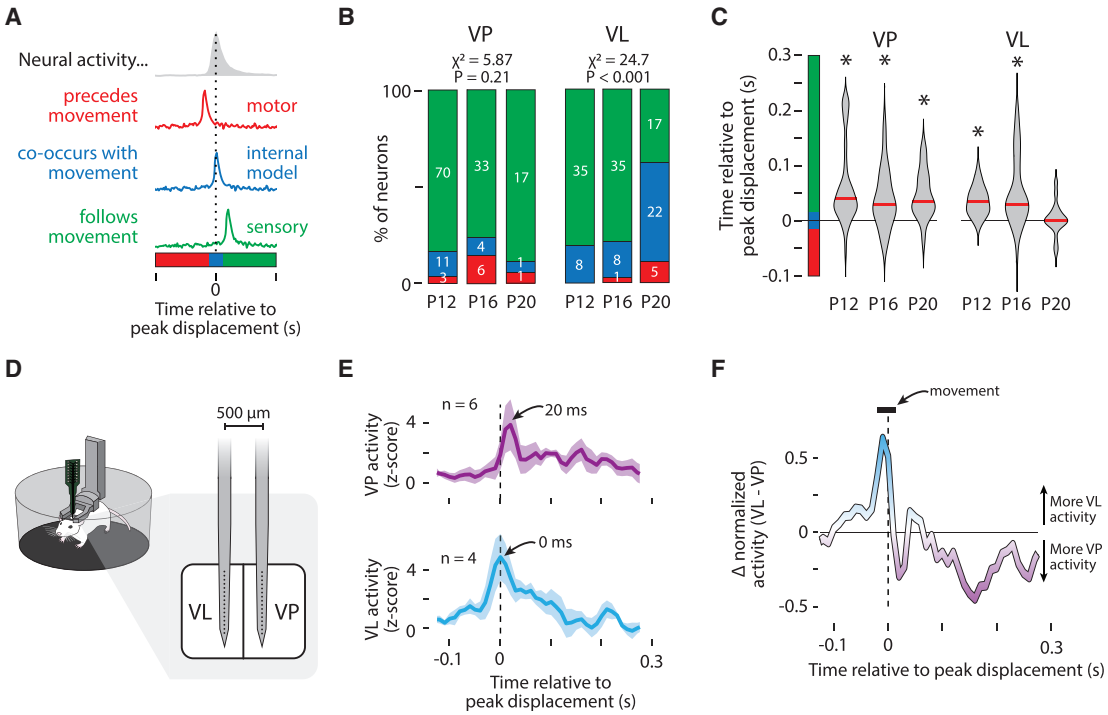

Figure 4. Diverging representations of movement in VP and VL

(A) Illustration of the possible temporal relationships between twitches and neural activity: motor (red); internal model (blue); and sensory (green).

(B) Percentage of neurons belonging to each category in (A). The number of neurons for each category is also shown. The percentage of neurons in each category is significantly different across age for VL ($p < 0.001$), but not VP.

(C) Violin plots of the time relative to peak displacement for VP (left) and VL (right) neurons at each age. Asterisks indicate that the median value (red line) is significantly different ($p < 0.0167$) from 0.

(D) Illustration of the electrode used to perform dual recordings in VL and VP in P20 rats.

(E) Mean (±SE) *Z*-scored neural activity of forelimb twitch-responsive neurons in VP (top) and VL (bottom) relative to peak forelimb displacement (dotted lines). Data are from one representative pup. The number of neurons contributing to each plot are shown.

(F) Difference between VL and VP activity as calculated from the normalized perievent histograms in (E), showing that VL exhibits more twitch-related activity than VP before peak displacement, whereas VP shows more twitch-related activity than VL after peak displacement (dotted line). The duration of the median movement (horizontal bar) is also shown.

See also Figure S4.

typically recorded neural activity while an animal repeats a movement dozens or hundreds of times.[9,14,16] Getting animals to repeat the same movement requires weeks of training, precluding investigation of when and how these representations develop. To circumvent this problem, we relied here on twitches, hundreds of which are produced discretely and spontaneously in a single recording session. Moreover, twitches exhibit remarkably consistent kinematics. Finally, because twitches are produced during the periods of muscle atonia that characterize active sleep, twitch-related reafference has a high signal-to-noise ratio.[45] These features of twitches enable direct comparison of movement-related activity across age, providing a window into the mechanisms by which neural representations of movement first emerge.

We found here that neural activity in VL co-occurs with movement, peaking 20–30 ms before activity in VP. Similarly timed activity has been found in VL across mammalian species. In primates, VL neurons respond faster than VP neurons to self-generated—but not other-generated—movements.[38,39] In rodents, VL shows rapid movement-related activity, although the timing of this activity has not been directly compared to sensory responses in VP.[9,13,14,16]

We also found here that cerebellar inactivation disrupts the timing of VL activity, paralleling similar findings in adult animals.[17,46] However, because previous studies have examined cerebellar activity as animals are producing complicated continuous movements (e.g., reaching for food), directly attributing neural activity in VL to any one facet of the movement has been challenging. Further complicating this issue, cerebellar inactivation can change the kinematics of the movements themselves.[13,17,47] Thus, although the cerebellum clearly shapes movement-related activity in VL, fully characterizing the cerebellum's contribution to this activity has remained elusive. Importantly, we found here that cerebellar inactivation did not change the kinematics of twitches (Figures S5G and S5H), thereby allowing us to directly compare movement-related activity in VL with and without cerebellar input. Upon inhibition of DCN activity, we observed a significant delay in movement-related activity that, we surmise, was caused by the blockade of biphasic DCN input to VL (Figure 6A, left). Consequently, by blocking

Please cite this article in press as: Dooley et al., Movements during sleep reveal the developmental emergence of a cerebellar-dependent internal model in motor thalamus, Current Biology (2021), https://doi.org/10.1016/j.cub.2021.10.014

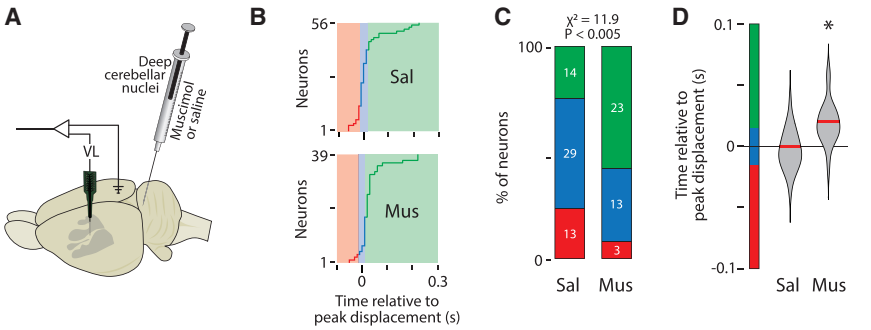

Figure 5. DCN inactivation at P20 disrupts VL activity

(A) Illustration of an infant rat brain to show the electrode locations and the microsyringe location in the DCN.

(B) Timing of peak neural activity relative to peak displacement for all twitch-responsive neurons in the saline (Sal; top) and muscimol (Mus; bottom) groups. Color codes are as in Figures 3A and 3B.

(C) Percentage of neurons in (B) belonging to each category in the Sal and Mus groups. The number of neurons for each category is also shown. The percentage of neurons in each category is significantly different between the two groups ($p < 0.005$).

(D) Violin plots of the time relative to peak displacement of VL neurons in the Sal and Mus groups. Asterisks indicate that the median value (red line) is significantly different from 0 ($p < 0.025$).

See also Figure S5.

DCN input to VL, we unmasked VL activity that arises from the sensory periphery (Figure 6A, right).

From the experimenter's point of view, it is relatively easy to attribute—with temporal precision—neural activity to twitches; conversely, it is quite difficult to attribute neural activity to individual facets of wake movements. This raises the intriguing possibility that, from a computational perspective, it might be easier for the developing cerebellum to detect—with temporal precision—the relationship between neural activity and twitches. If we take this possibility seriously, it suggests that twitches play a unique role in the development of internal models. Even if so, it remains possible that the development of internal models of movement described here is specific to twitches and that the development of such models for other types of movement is a separate process. However, given that the same neurons in VL showed movement-related activity for twitches and wake movements (Figure 2), we find it more likely that these early-developing internal models will contribute to functional wake movements as well.

Is the P20 cerebellum a Smith Predictor?

Applying the principles of mechanical engineering to neuroscience, Miall and colleagues[48] hypothesized that the cerebellum functions as a predictive controller called a Smith Predictor. A Smith Predictor comprises two internal models: (1) a simple forward model that mimics the timing of a self-generated movement, enabling prediction of the expected sensory consequences of movement, and (2) a lagged inhibitory copy of the original forward model that accounts for feedback delays in the system (e.g., conduction delays from muscle to brain). When the actual and predicted sensory feedback signals match, they cancel each other out, resulting in no change in overall activity (Figure 6A, left). We propose that, by P20, the biphasic cerebellar input to VL functions as a Smith Predictor (Figure 6B). Accordingly, without cerebellar input to VL, its activity (like that of VP) would predominantly reflect sensory input, as found here.

Previous research supports the above interpretation. In adult rats, DCN neurons show a biphasic response to whisker movements, composed of an early burst of activity at movement onset followed by a longer decrease in activity that results from DCN inhibition by Purkinje cells.[49] Further, in P8 rats, copies of motor commands, including those that produce twitches, are conveyed from the red nucleus and adjacent neurons to precerebellar nuclei (i.e., the inferior olive and lateral reticular nucleus), before projecting to the cerebellum via climbing and mossy fibers.[20] Also, as demonstrated in P8 and P12 rats, both Purkinje cells and the DCN exhibit clear twitch-related activity.[43,50,51] Thus, we propose that a biphasic response in VL results from two temporally segregated signals from the DCN: an early response that reflects forward-model computations built upon motor copies arising from precerebellar nuclei and a late response that reflects the lagged inhibitory

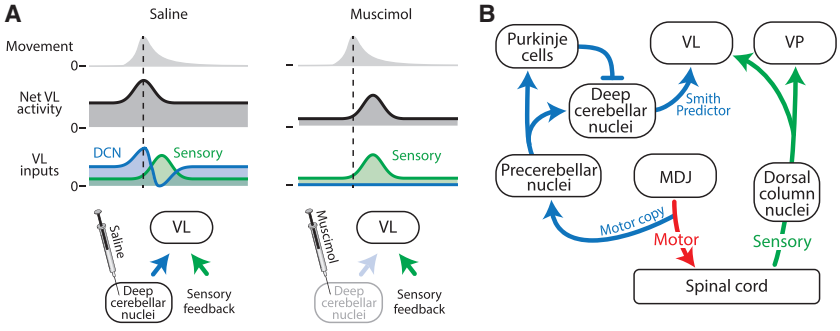

Figure 6. Cerebellar and sensory inputs differentially drive VL activity

(A) Proposed model explaining twitch-related VL activity in the Sal (left) and Mus (right) groups. In Sal-injected pups, VL receives input from the DCN (blue) and sensory feedback (green). Early activity from the DCN (blue peak) provides VL with a forward model of the twitch, and the later decrease in activity (blue trough) cancels the sensory signal (green peak). In Mus-injected pups, both the early- and the late-arriving signals from the DCN are blocked, thereby revealing the sensory feedback signal.

(B) Circuit diagram to support the functional hypothesis in (A). Separate pathways are shown for motor signals (red), sensory signals (green), and signals that convey a Smith Predictor to VL (blue). MDJ, mesodiencephalic junction.

copy that arises from inhibition of the DCN by Purkinje cells (Figure 6B).

Movements during active sleep are ideally suited to calibrate a Smith Predictor

The establishment and maintenance of a functioning Smith Predictor relies heavily on accurate timing: to properly cancel the actual sensory feedback from a movement, the delayed inhibition of reafference must precisely match the conduction delay of the reafferent signal. Further complicating this issue, changes in myelination and axonal length during bodily growth and development will modify the conduction delays of sensory feedback.[52] Accordingly, this system cannot be prespecified or genetically programmed. It must develop.

Miall and colleagues were aware of this problem and proposed a potential solution: "The size of the feedback time delay could be estimated by measuring the delay between issuing a motor command and assessing its result. This would be most easy to do if the motor command were discrete…, for the reafferent signal would then change abruptly."[48] Twitches are exactly this type of discrete signal. In other words, Miall and colleagues foreshadowed a solution, based on design principles, that is readily available as a naturally occurring behavior in infant animals. Moreover, given the present demonstration that twitches drive neural activity in thalamic and cortical structures far beyond the period of early infancy, we propose that twitches continue to calibrate the sensorimotor system across the lifespan to enable precise predictions of the expected delays of reafference from wake movements. In this way, the distinct kinematic features of movements during sleep and wake can be viewed as complementary modes of activation for the sensorimotor system.

STAR★METHODS

Detailed methods are provided in the online version of this paper and include the following:

- KEY RESOURCES TABLE
- RESOURCE AVAILABILITY
  - Lead contact
  - Materials availability
  - Data and code availability
- EXPERIMENTAL MODEL AND SUBJECT DETAILS
- METHOD DETAILS
  - Surgery
  - Recording Environment
  - Electrophysiological Recordings
  - DCN Injections
  - Video Collection and Synchronization
  - Histology
  - Classification of Behavioral State
  - Classification of Movement
  - Local Field Potential
  - Spike Sorting
- QUANTIFICATION AND STATISTICAL ANALYSIS
  - Determination of Twitch-Responsiveness
  - Movement Analysis
  - Width at Half- and Three-Quarter-Height
  - Statistical Analyses

SUPPLEMENTAL INFORMATION

Supplemental information can be found online at https://doi.org/10.1016/j.cub.2021.10.014.

ACKNOWLEDGMENTS

We thank Ryan Glanz for technical assistance. This research was supported by grants from the National Institutes of Health (R37-HD081168 to M.S.B. and F32-NS101858 to J.C.D.).

AUTHOR CONTRIBUTIONS

Conceptualization, J.C.D., G.S., and M.S.B.; methodology, J.C.D., G.S., and M.S.B.; software, J.C.D.; formal analysis, J.C.D.; investigation, J.C.D.; data curation, J.C.D.; writing – original draft, J.C.D. and M.S.B.; writing – review & editing, J.C.D., G.S., and M.S.B.; visualization, J.C.D., G.S., and M.S.B.; funding acquisition, J.C.D., G.S., and M.S.B.; resources, G.S. and M.S.B.; supervision, G.S. and M.S.B.

DECLARATION OF INTERESTS

The authors declare no competing interests.

Received: July 21, 2021
Revised: September 6, 2021
Accepted: October 6, 2021
Published: November 1, 2021

REFERENCES

1. Ebbesen, C.L., Insanally, M.N., Kopec, C.D., Murakami, M., Saiki, A., and Erlich, J.C. (2018). More than just a "motor": recent surprises from the frontal cortex. J. Neurosci. *38*, 9402–9413.
2. Sathyamurthy, A., Barik, A., Dobrott, C.I., Matson, K.J.E., Stoica, S., Pursley, R., Chesler, A.T., and Levine, A.J. (2020). Cerebellospinal neurons regulate motor performance and motor learning. Cell Rep. *31*, 107595.
3. Brooks, J.X., and Cullen, K.E. (2019). Predictive sensing: the role of motor signals in sensory processing. Biol. Psychiatry Cogn. Neurosci. Neuroimaging *4*, 842–850.
4. Hull, C. (2020). Prediction signals in the cerebellum: beyond supervised motor learning. eLife *9*, e54073.
5. Bastian, A.J. (2006). Learning to predict the future: the cerebellum adapts feedforward movement control. Curr. Opin. Neurobiol. *16*, 645–649.
6. Crapse, T.B., and Sommer, M.A. (2008). Corollary discharge across the animal kingdom. Nat. Rev. Neurosci. *9*, 587–600.
7. Franklin, D.W., and Wolpert, D.M. (2011). Computational mechanisms of sensorimotor control. Neuron *72*, 425–442.
8. Bosch-Bouju, C., Hyland, B.I., and Parr-Brownlie, L.C. (2013). Motor thalamus integration of cortical, cerebellar and basal ganglia information: implications for normal and parkinsonian conditions. Front. Comput. Neurosci. *7*, 163.
9. Sauerbrei, B.A., Guo, J.Z., Cohen, J.D., Mischiati, M., Guo, W., Kabra, M., Verma, N., Mensh, B., Branson, K., and Hantman, A.W. (2020). Cortical pattern generation during dexterous movement is input-driven. Nature *577*, 386–391.
10. Habas, C., Manto, M., and Cabaraux, P. (2019). The cerebellar thalamus. Cerebellum *18*, 635–648.
11. Wolpert, D.M., Miall, R.C., and Kawato, M. (1998). Internal models in the cerebellum. Trends Cogn. Sci. *2*, 338–347.
12. Gornati, S.V., Schäfer, C.B., Eelkman Rooda, O.H.J., Nigg, A.L., De Zeeuw, C.I., and Hoebeek, F.E. (2018). Differentiating cerebellar impact on thalamic nuclei. Cell Rep. *23*, 2690–2704.
13. Dacre, J., Colligan, M., Clarke, T., Ammer, J.J., Schiemann, J., Chamosa-Pino, V., Claudi, F., Harston, J.A., Eleftheriou, C., Pakan, J.M.P., et al.

(2021). A cerebellar-thalamocortical pathway drives behavioral context-dependent movement initiation. Neuron *109*, 2326–2338.e8.

14. Bosch-Bouju, C., Smither, R.A., Hyland, B.I., and Parr-Brownlie, L.C. (2014). Reduced reach-related modulation of motor thalamus neural activity in a rat model of Parkinson's disease. J. Neurosci. *34*, 15836–15850.
15. Wagner, M.J., Kim, T.H., Kadmon, J., Nguyen, N.D., Ganguli, S., Schnitzer, M.J., and Luo, L. (2019). Shared cortex-cerebellum dynamics in the execution and learning of a motor task. Cell *177*, 669–682.e24.
16. Gaidica, M., Hurst, A., Cyr, C., and Leventhal, D.K. (2018). Distinct populations of motor thalamic neurons encode action initiation, action selection, and movement vigor. J. Neurosci. *38*, 6563–6573.
17. Nashef, A., Cohen, O., Harel, R., Israel, Z., and Prut, Y. (2019). Reversible block of cerebellar outflow reveals cortical circuitry for motor coordination. Cell Rep. *27*, 2608–2619.e4.
18. Blumberg, M.S., Coleman, C.M., Gerth, A.I., and McMurray, B. (2013). Spatiotemporal structure of REM sleep twitching reveals developmental origins of motor synergies. Curr. Biol. *23*, 2100–2109.
19. Blumberg, M.S., Dooley, J.C., and Sokoloff, G. (2020). The developing brain revealed during sleep. Curr. Opin. Physiol. *15*, 14–22.
20. Mukherjee, D., Sokoloff, G., and Blumberg, M.S. (2018). Corollary discharge in precerebellar nuclei of sleeping infant rats. eLife *7*, e38213.
21. Altman, J. (1969). Autoradiographic and histological studies of postnatal neurogenesis. 3. Dating the time of production and onset of differentiation of cerebellar microneurons in rats. J. Comp. Neurol. *136*, 269–293.
22. Watanabe, M., and Kano, M. (2011). Climbing fiber synapse elimination in cerebellar Purkinje cells. Eur. J. Neurosci. *34*, 1697–1710.
23. Freeman, J.H., Jr., and Nicholson, D.A. (2004). Developmental changes in the neural mechanisms of eyeblink conditioning. Behav. Cogn. Neurosci. Rev. *3*, 3–13.
24. Nicholson, D.A., and Freeman, J.H., Jr. (2003). Addition of inhibition in the olivocerebellar system and the ontogeny of a motor memory. Nat. Neurosci. *6*, 532–537.
25. Freeman, J.H., Jr., and Nicholson, D.A. (2000). Developmental changes in eye-blink conditioning and neuronal activity in the cerebellar interpositus nucleus. J. Neurosci. *20*, 813–819.
26. Jouvet-Mounier, D., Astic, L., and Lacote, D. (1970). Ontogenesis of the states of sleep in rat, cat, and guinea pig during the first postnatal month. Dev. Psychobiol. *2*, 216–239.
27. Frank, M.G., and Heller, H.C. (1997). Development of REM and slow wave sleep in the rat. Am. J. Physiol. *272*, R1792–R1799.
28. Gramsbergen, A., Schwartze, P., and Prechtl, H.F.R. (1970). The postnatal development of behavioral states in the rat. Dev. Psychobiol. *3*, 267–280.
29. Singleton, A.C., Brown, A.R., and Teskey, G.C. (2021). Development and plasticity of complex movement representations. J. Neurophysiol. *125*, 628–637.
30. Young, N.A., Vuong, J., and Teskey, G.C. (2012). Development of motor maps in rats and their modulation by experience. J. Neurophysiol. *108*, 1309–1317.
31. Dooley, J.C., and Blumberg, M.S. (2018). Developmental 'awakening' of primary motor cortex to the sensory consequences of movement. eLife *7*, e41841.
32. Gómez, L.J., Dooley, J.C., Sokoloff, G., and Blumberg, M.S. (2021). Parallel and serial sensory processing in developing primary somatosensory and motor cortex. J. Neurosci. *41*, 3418–3431.
33. Colonnese, M.T., Kaminska, A., Minlebaev, M., Milh, M., Bloem, B., Lescure, S., Moriette, G., Chiron, C., Ben-Ari, Y., and Khazipov, R. (2010). A conserved switch in sensory processing prepares developing neocortex for vision. Neuron *67*, 480–498.
34. Murata, Y., and Colonnese, M.T. (2018). Thalamus controls development and expression of arousal states in visual cortex. J. Neurosci. *38*, 8772–8786.
35. Ebner, F.F., and Kaas, J.H. (2015). Somatosensory System (Elsevier), pp. 675–701.
36. Asanuma, H., and Mackel, R. (1989). Direct and indirect sensory input pathways to the motor cortex; its structure and function in relation to learning of motor skills. Jpn. J. Physiol. *39*, 1–19.
37. Berkley, K.J. (1983). Spatial relationships between the terminations of somatic sensory motor pathways in the rostral brainstem of cats and monkeys. II. Cerebellar projections compared with those of the ascending somatic sensory pathways in lateral diencephalon. J. Comp. Neurol. *220*, 229–251.
38. Butler, E.G., Horne, M.K., and Hawkins, N.J. (1992). The activity of monkey thalamic and motor cortical neurones in a skilled, ballistic movement. J. Physiol. *445*, 25–48.
39. Butler, E.G., Horne, M.K., and Rawson, J.A. (1992). Sensory characteristics of monkey thalamic and motor cortex neurones. J. Physiol. *445*, 1–24.
40. Makous, J.C., Friedman, R.M., and Vierck, C.J., Jr. (1996). Effects of a dorsal column lesion on temporal processing within the somatosensory system of primates. Exp. Brain Res. *112*, 253–267.
41. Lund, R.D., and Webster, K.E. (1967). Thalamic afferents from the dorsal column nuclei. An experimental anatomical study in the rat. J. Comp. Neurol. *130*, 301–312.
42. Manto, M., and Oulad Ben Taib, N. (2010). Cerebellar nuclei: key roles for strategically located structures. Cerebellum *9*, 17–21.
43. Del Rio-Bermudez, C., Plumeau, A.M., Sattler, N.J., Sokoloff, G., and Blumberg, M.S. (2016). Spontaneous activity and functional connectivity in the developing cerebellorubral system. J. Neurophysiol. *116*, 1316–1327.
44. Quy, P.N., Fujita, H., Sakamoto, Y., Na, J., and Sugihara, I. (2011). Projection patterns of single mossy fiber axons originating from the dorsal column nuclei mapped on the aldolase C compartments in the rat cerebellar cortex. J. Comp. Neurol. *519*, 874–899.
45. Blumberg, M.S., Marques, H.G., and Iida, F. (2013). Twitching in sensorimotor development from sleeping rats to robots. Curr. Biol. *23*, R532–R537.
46. Nashef, A., Cohen, O., Israel, Z., Harel, R., and Prut, Y. (2018). Cerebellar shaping of motor cortical firing is correlated with timing of motor actions. Cell Rep. *23*, 1275–1285.
47. Becker, M.I., and Person, A.L. (2019). Cerebellar control of reach kinematics for endpoint precision. Neuron *103*, 335–348.e5.
48. Miall, R.C., Weir, D.J., Wolpert, D.M., and Stein, J.F. (1993). Is the cerebellum a smith predictor? J. Mot. Behav. *25*, 203–216.
49. Brown, S.T., and Raman, I.M. (2018). Sensorimotor integration and amplification of reflexive whisking by well-timed spiking in the cerebellar corticonuclear circuit. Neuron *99*, 564–575.e2.
50. Sokoloff, G., Plumeau, A.M., Mukherjee, D., and Blumberg, M.S. (2015). Twitch-related and rhythmic activation of the developing cerebellar cortex. J. Neurophysiol. *114*, 1746–1756.
51. Sokoloff, G., Uitermarkt, B.D., and Blumberg, M.S. (2015). REM sleep twitches rouse nascent cerebellar circuits: implications for sensorimotor development. Dev. Neurobiol. *75*, 1140–1153.
52. Downes, N., and Mullins, P. (2014). The development of myelin in the brain of the juvenile rat. Toxicol. Pathol. *42*, 913–922.
53. Domínguez, S., Ma, L., Yu, H., Pouchelon, G., Mayer, C., Spyropoulos, G.D., Cea, C., Buzsáki, G., Fishell, G., Khodagholy, D., and Gelinas, J.N. (2021). A transient postnatal quiescent period precedes emergence of mature cortical dynamics. eLife *10*, e69011.
54. Szymusiak, R., and Satinoff, E. (1981). Maximal REM sleep time defines a narrower thermoneutral zone than does minimal metabolic rate. Physiol. Behav. *26*, 687–690.
55. Dooley, J.C., Glanz, R.M., Sokoloff, G., and Blumberg, M.S. (2020). Self-generated whisker movements drive state-dependent sensory input to developing barrel cortex. Curr. Biol. *30*, 2404–2410.e4.

56. Cox, C.L., Huguenard, J.R., and Prince, D.A. (1996). Heterogeneous axonal arborizations of rat thalamic reticular neurons in the ventrobasal nucleus. J. Comp. Neurol. *366*, 416–430.

57. Seelke, A.M., Dooley, J.C., and Krubitzer, L.A. (2012). The emergence of somatotopic maps of the body in S1 in rats: the correspondence between functional and anatomical organization. PLoS ONE *7*, e32322.

58. Seelke, A.M., and Blumberg, M.S. (2008). The microstructure of active and quiet sleep as cortical delta activity emerges in infant rats. Sleep *31*, 691–699.

59. Gervasoni, D., Lin, S.C., Ribeiro, S., Soares, E.S., Pantoja, J., and Nicolelis, M.A. (2004). Global forebrain dynamics predict rat behavioral states and their transitions. J. Neurosci. *24*, 11137–11147.

60. Pachitariu, M., Steinmetz, N., Kadir, S., Carandini, M., and Kenneth, D.H. (2016). Kilosort: realtime spike-sorting for extracellular electrophysiology with hundreds of channels. bioRxiv, 061481.

61. Rossant, C., and Harris, K.D. (2013). Hardware-accelerated interactive data visualization for neuroscience in Python. Front. Neuroinform. *7*, 36.

Please cite this article in press as: Dooley et al., Movements during sleep reveal the developmental emergence of a cerebellar-dependent internal model in motor thalamus, Current Biology (2021), https://doi.org/10.1016/j.cub.2021.10.014

STAR★METHODS

KEY RESOURCES TABLE

REAGENT or RESOURCE	SOURCE	IDENTIFIER
Chemicals, peptides, and recombinant proteins		
Vybrant Dil Cell-Labeling Solution	Life Technologies	Cat #: V22885
Muscimol	Sigma-Aldrich	CAS #: 2763-96-4
Cresyl violet acetate	MP Biomedicals	Cat #: 02150727
Isoflurane	Phoenix Pharmaceuticals	Item #: 0010250
Ketamine hydrochloride	Akorn Animal Health	NDC: 59399-114-10
Xylazine	Lloyd Laboratories	sc-362949Rx
3,3′-Diaminobenzidine Tetrahydrochloride	Spectrum	TCI-D0078-5G
Catalase from bovine liver	Sigma-Aldrich	C9322
Cytochrome *c* from equine heart	Sigma-Aldrich	C2506
Fluorogold	Fluorochrome	https://fluorochrome.com
Carprophen	Putney	#200-522
Bupivacaine	Pfizer	NDC 0409-1162-19
Vetbond	3M	https://www.3m.com
1.8 mm Trephine	Fine Science Tools	Item #: 18004-18
Experimental models: Organisms/strains		
Sprague-Dawley Norway Rats	Envigo	RRID: RGD_10401918
Software and algorithms		
MATLAB, version 2020b	Mathworks	RRID: SCR_001622
Spike2 Software, version 8	Cambridge Electronic Design	RRID: SCR_000903
Adobe Illustrator Creative Cloud 2021	Adobe	RRID: SCR_010279
Adobe Photoshop Creative Cloud 2021	Adobe	RRID: SCR_014199
Image Composite Editor 2.0	Microsoft	https://www.microsoft.com/
Other		
Stereotaxic apparatus	David Kopf Instruments	Model: 900
Multi-probe micromanipulator system	New Scale Techologies	Custom
Mobile HomeCage	Neurotar	MHC-S-T
Headplate	Neurotar	Custom
Freezing microtome	Leica	Model: SM2000 R
Fluorescent microscope	Leica	DM6b/DMC7000T
Stainless steel ground wire	California Fine Wire Company	Cat #: M311490
Stainless steel EMG wire	California Fine Wire Company	Cat #: M408090
Microsyringe	Hamilton Company	Product Number 65458-02
LabRat	Tucker-Davis Technologies	LR10
Recording electrodes	NeuroNexus	A16-3mm-100-177; A16-10mm-100-177; A2x16-10mm-50-500-177
Electrophysiological, behavioral, and displacement data	Dryad	https://doi.org/10.5061/dryad.08kprr53d

RESOURCE AVAILABILITY

Lead contact

Further information and requests for resources should be directed to, and will be fulfilled by, the lead contact, Dr. James Dooley (james-c-dooley@uiowa.edu).

Materials availability

This study did not generate new unique reagents.

Please cite this article in press as: Dooley et al., Movements during sleep reveal the developmental emergence of a cerebellar-dependent internal model in motor thalamus, Current Biology (2021), https://doi.org/10.1016/j.cub.2021.10.014

Data and code availability

Electrophysiological spiking data, timecodes for twitches and wake movements, as well as displacement data for each animal have been deposited at Dryad and are publicly available as of the date of publication. DOIs are listed in the Key resources table.

All original code has been deposited at https://github.com/jcdooley/Dooley_et_al_2021 and is publicly available as of the date of publication. DOIs are listed in the Key resources table.

Any additional information required to reanalyze the data reported in this paper is available from the lead contact upon request.

EXPERIMENTAL MODEL AND SUBJECT DETAILS

For the first experiment, cortical and thalamic activity was recorded from Sprague-Dawley Norway rats (*Rattus norvegicus*) at P12 (N = 11 pups; 31.0 ± 2.1 g; 3 male), P15-16 (hereafter P16; N = 12 pups; 44.0 ± 3.1 g; 8 male), and P19-23 (hereafter P20; N = 22 pups; 61.6 ± 7.6 g; 15 male). Animals within the same age group were always selected from different litters. Recordings were performed in the forelimb region of M1 and either the ventral lateral (VL) or the ventral posterior (VP) nucleus of thalamus. For an animal to be included in the analysis, it needed more than 40 twitches of a single body part and at least one neuron had to be classified as twitch responsive, criteria that lead to the exclusion of 8 animals. An additional 3 rats were used at P20 for dual recordings in VL and VP. For the experiment in which the deep cerebellar nuclei (DCN) were inactivated, a total of 12 male and female P20 rats were used (n = 6 per group).

Pups were born and reared in standard laboratory cages (48 × 20 × 26 cm) in a temperature- and humidity-controlled room on a 12:12 light-dark cycle, with food and water available *ad libitum*. The day of birth was considered P0 and litters were culled to eight pups by P3. All pups had at least four littermates until P12 and at least two littermates on the day that neurophysiological recordings were performed. No pups were weaned before testing. All experiments were conducted in accordance with the National Institutes of Health (NIH) Guide for the Care and Use of Laboratory Animals (NIH Publication No. 80–23) and were approved by the Institutional Animal Care and Use Committee of the University of Iowa.

METHOD DETAILS

Surgery

As described previously,[31] a pup with a visible milk band (P12) or a healthy body weight (P16 and P20) was removed from the litter and anesthetized with isoflurane gas (3%–5%; Phoenix Pharmaceuticals, Burlingame, CA). The hair on the top of the head was shaved and care was taken to ensure that the vibrissae were intact. Two custom-made bipolar hook electrodes (0.002 inch diameter, epoxy coated; California Fine Wire, Grover Beach, CA) were inserted into the nuchal and biceps muscles contralateral to the neural recordings for state determination. Carprofen (5 mg/kg SC; Putney, Portland, ME) was administered as an anti-inflammatory analgesic.

The skin above the skull was carefully removed and an analgesic (bupivicane; Pfizer, New York, NY) was applied topically to the skull. The skull was then dried with bleach. For P20 rats, any bleeding around the skull was cauterized to ensure that it was completely dry. Vetbond (3M, Minneapolis, MN) was then applied to the skin surrounding the incision, and a custom-manufactured head-plate (Neurotar, Helsinki, Finland) was secured to the skull using cyanoacrylate adhesive.

A trephine drill (1.8 mm; Fine Science Tools, Foster City, CA) was used to drill a hole into the skull above the forelimb representation of M1 (0.5 mm anterior to bregma, 2.2–2.5 mm lateral to the sagittal suture) and either VL (2.0–2.2 mm caudal to bregma, 2.2 mm lateral to the sagittal suture) or VP (2.5–2.8 mm caudal to bregma, 2.5 mm lateral to the sagittal suture). For cerebellar injections, a third hole was drilled above the DCN (3.5 mm caudal to lambda, 2–2.2 mm lateral, contralateral to the other two holes). Care was taken to not puncture the underlying dura matter. A small amount of peanut oil was applied to the dura to prevent desiccation of the underlying tissue. This surgical procedure lasted approximately 30 min.

While recovering from anesthesia, the pup was secured to a custom-made head-fixation block secured to a Mobile HomeCage (NTR000289-01; Neurotar). The height of the pup's head off the floor was adjusted depending on its age so that, when the pup was exhibiting atonia during active sleep, its body rested on its elbows (P12: 35 mm; P16: 38 mm; P20: 40 mm). EMG wires were carefully secured to ensure they were out of reach of the animal. Pups recovered from anesthesia within 15 minutes and were acclimated to the head-fix apparatus for 1 to 2.5 hours. This period of acclimation allowed the recording electrodes to stabilize and the return of normal spiking activity.[53] Also, when recording began, all pups were exhibiting typical behavioral and electrophysiological features of sleep and wake (i.e., twitching, grooming, locomotion).

Recording Environment

Electrophysiological recordings were performed in a Faraday cage illuminated by flicker-free red LEDs (630 nm; Waveform Lighting, Vancouver, WA). Continuous white noise (70 dB) was present throughout the recording session. To maximize REM sleep, the room's temperature was maintained between 26.5 and 29°C.[54] The animal's head was positioned away from the entry to the room so that it could not see the experimenter entering or leaving, which was infrequent; whenever possible, the experimenter was outside the room and monitoring the animal and data collection remotely.

Electrophysiological Recordings

The nuchal and biceps EMG electrodes were connected to the analog inputs of a Lab Rat LR-10 acquisition system (Tucker Davis Technologies, Gainesville, FL). The EMG signals were sampled at approximately 1.5 kHz and high-pass filtered at 300 Hz.

Please cite this article in press as: Dooley et al., Movements during sleep reveal the developmental emergence of a cerebellar-dependent internal model in motor thalamus, Current Biology (2021), https://doi.org/10.1016/j.cub.2021.10.014

Before insertion, we coated the two 16-channel silicon depth electrodes (A1x16-3mm-100-177-A16 or A1x16-10mm-100-177-A16, depending on the depth of the recording site) or one 32-channel electrode (A2x16-10mm-50-500-177-A16) with fluorescent DiI (Vybrant DiI Cell-Labeling Solution; Life Technologies, Grand Island, NY). Electrodes were inserted using a multiprobe manipulator (New Scale Technologies; Victor, NY) controlled by an Xbox controller (Microsoft, Redmond, WA). For M1 recordings, the electrode was inserted tangentially to the cortical surface until all electrode sites were beneath the dura (approximately 1500 μm). For thalamic recordings, the electrode was inserted to a depth ranging from 4500 to 5800 μm, until neurons from VL or VP—which were much more active than neurons in surrounding areas—were centered on the electrode. A chlorinated Ag/Ag-Cl wire (0.25 mm diameter; Medwire, Mt. Vernon, NY) inserted into occipital cortex contralateral to the cortical and thalamic recording sites, served as both reference and ground. Neural signals were sampled at approximately 25 kHz, and both a high-pass filter (0.1 Hz) and a harmonic notch filter (60, 120, and 180 Hz) was applied.

Electrophysiological data were acquired continuously for 3-6 h using SynapseLite (Tucker Davis Technologies). The Mobile HomeCage enabled stable head-fixation while rats were able to locomote, groom, and sleep throughout the recording session.

DCN Injections

Pups were prepared for testing as described above. In addition, a microsyringe (1 μL; Hamilton, Reno, NV), angled 8° caudally, was inserted into the DCN contralateral to VL recordings and ipsilateral to the behaviorally scored limbs and whiskers (see Figure 5A). The recording session began with a 60-min baseline period followed by a 15-min diffusion period and a 240-min recording period. A total volume of 0.5 μL of fluorophore-conjugated muscimol (1.6 mM; Sigma-Aldrich, St. Louis, MO) or saline was injected at a rate of 0.1 μL/min.

Video Collection and Synchronization

As described previously,[55] video data were synchronized to electrophysiological recordings so that we could better quantify movements and behavioral state. Rats were surrounded by a clear enclosure within the Mobile HomeCage, enabling unimpeded visual access. Video was recorded using a single Blackfly-S camera (FLIR Integrated Systems; Wilsonville, OR) positioned at a 45° angle (relative to the pup's head) and centered on the right forelimb, contralateral to cortical and thalamic recordings. This angle provided an unobstructed view of the right whiskers, forelimb, hindlimb, and tail. Video was collected in SpinView (FLIR Integrated Systems) at 100 frames/s, with a 7 ms exposure time and 720 × 540 pixel resolution.

Video frames were synchronized to the electrophysiological record using an external time-locking stimulus. A red LED, controlled by SynapseLite (Tucker Davis Technologies), was in view of the camera and pulsed every 3 s for a duration of 100 ms. Custom MATLAB scripts determined the number of frames between each LED pulse to check for dropped frames. Although infrequent, when the number of frames between pulses was not equal to 300 (3 s inter-pulse interval x 100 frames/s), a "dummy frame" was inserted in that location. This ensured that the video and electrophysiological data were synchronized to within 10 ms throughout the recording session.

Histology

At the end of the recording session, the pup was euthanized with ketamine/xylazine (10:1; > 0.08 mg/kg) and perfused with 0.1 M phosphate-buffered saline (PBS) followed by 4% paraformaldehyde (PFA). The brain was extracted and post-fixed in 4% PFA for at least 24 h and was then transferred to a 30% sucrose solution at least 24 h before sectioning.

To confirm the electrode's location in M1, the brain was either flattened and sectioned tangentially to the pial surface or sectioned coronally. When sectioned tangentially, the right cortical hemisphere was dissected from the subcortical tissue and flattened between two glass slides (separated using a 1.5 mm spacer) for 5-15 min. Small weights (10 g) applied light pressure to the upper slide. To visualize thalamic and cerebellar tissue, brains were always sectioned coronally. Regardless of the plane of section, the tissue was sectioned at 80 μm. Wet-mounted sections were imaged at 2.5x using a fluorescent microscope and digital camera (Leica Microsystems, Buffalo Grove, IL) to identify the location of the DiI.

Cortical and thalamic sections were stained for cytochrome oxidase (CO), which reliably delineates primary sensory areas in cortex and nuclei in thalamus, including VP and VL, at these ages.[56,57] Briefly, cytochrome C (3 mg per 10 mL solution; Sigma-Aldrich), catalase (2 mg per 10 mL solution; Sigma-Aldrich) and 3,3′-diaminobenzidine tetrahydrochloride (DAB; 5 mg per 10 mL solution; Spectrum, Henderson, NV) were dissolved in a 1:1 dilution of PB-H_2O and distilled water. Sections were developed in well plates on a shaker at 35–40°C at approximately 100 rotations per min for 3–6 h, after which they were washed and mounted and allowed at least 48 h to dry. Once dry, sections were placed in citrus clearing solution and coverslipped.

Cerebellar sections were stained for Nissl, which reliably shows the boundaries of the interposed, dentate, and fastigial nuclei by P12.[43] Briefly, cerebellar sections were mounted directly to gelatin-dipped slides and allowed to dry for at least 48 h. Next, sections were rehydrated in distilled H_2O and soaked in cresyl violet for 45 min. They were then rinsed in deionized H_2O and transferred to a solution composed of 75% ethanol, 24.5% deionized H_2O, and 0.5% acetic acid. Sections were checked several times per minute until they had sufficiently bleached, and then rinsed for three min in progressively higher concentrations of ethanol, placed in citrus clearing solution, and coverslipped.

Stained sections were photographed at 2.5x or 5x magnification. Multiple photographs were combined into a single composite image (Microsoft Image Composite Editor) and the electrode or needle location, as well as drug diffusion, were visualized in relation to areal, nuclear, and laminar boundaries of the stained tissue.

Please cite this article in press as: Dooley et al., Movements during sleep reveal the developmental emergence of a cerebellar-dependent internal model in motor thalamus, Current Biology (2021), https://doi.org/10.1016/j.cub.2021.10.014

Classification of Behavioral State

As described previously, behavior, nuchal EMG signals, and cortical LFP were used to identify periods of wake, active sleep, and quiet sleep.[58] Wake was characterized by periods of high nuchal muscle tone and wake-related behaviors (e.g., locomotion, grooming). Active sleep was characterized by the occurrence of myoclonic twitches against a background of muscle atonia. At P16 and P20, active sleep was also accompanied by continuous theta oscillations in thalamus (see Figure 1D).[59] During quiet sleep, we observed high cortical delta power, behavioral quiescence, and moderate nuchal muscle tone (see Figure 1D), although periods of high delta power were sometimes accompanied by nuchal muscle atonia. Periods not assigned as active or quiet sleep were designated as wake. Active wake was defined as that part of the wake period that was within 3 s of a movement.

Classification of Movement

As described previously,[55] to quantify periods of movement, we used custom MATLAB scripts to detect frame-by-frame changes in pixel intensity within regions-of-interest (ROIs). The number of pixels within the ROI that exhibited an intensity change > 5% were summed. This calculation was performed for each frame, resulting in a time series of quantified movement.

For twitches, the movement timeseries for an ROI containing the body part of interest (e.g., forelimb) was visualized alongside the video using Spike2 (Version 8; Cambridge Electronic Design, Cambridge, UK). Peaks in the timeseries were confirmed to be twitches of the appropriate body part. Twitch onset was defined as the first frame in which movement occurred (as determined by a change in intensity in the ROI). For the forelimb, hindlimb, and tail, this method effectively counted every visible twitch, since even twitches in rapid succession have distinct onset and offset times. However, for whisker twitches, alternating protractions and retractions did not always have clear temporal boundaries, thus making it difficult to determine when one whisker twitch ended and another began. In these instances, only the first whisker twitch in a series of twitches was counted.

For wake movements, an ROI of the entire animal was used. Because multiple wake movements typically occur in quick succession, it was often the case that only the first wake movement in a bout could be used. Thus, our quantification of wake movements underestimates the total number of movements produced.

Local Field Potential

For all local field potential analyses, the raw neural signal was down sampled to ~1000 Hz and smoothed using a moving Gaussian kernel with a half-width of 0.5 ms.

Spike Sorting

SynapseLite files were converted to binary files using custom MATLAB scripts and sorted with Kilosort2.[60] Briefly, data were whitened (covariance-standardized) and band-pass filtered (300-5000 Hz) before spike detection. Template-matching was implemented to sort the event waveforms into clusters. The first-pass spike detection threshold was set to six standard deviations below the mean and the second-pass threshold was set to five standard deviations below the mean. The minimum allowable firing rate was set to 0.01 spikes/s and the bin size for template detection was set to 262,400 sample points, or approximately 11 s. All other Kilosort2 parameters were left at default values.

Clusters were visualized and sorted in Phy2.[61] Putative single units had spike waveforms that reliably fit within a well-isolated waveform template, appeared in a principal component analysis as a distinct cluster, and had an auto-correlogram with a decreased firing rate at a time lag of 0 (indicative of a unit's refractory period).

Clusters meeting the first two criteria but not the third were considered multi-units and were discarded from analysis. Any putative unit with a waveform template indicative of electrical noise, a firing rate < 0.01 spikes/s, or amplitude drift across the recording period was discarded.

QUANTIFICATION AND STATISTICAL ANALYSIS

Determination of Twitch-Responsiveness

All analyses of neural data were performed in MATLAB using custom-written scripts. The relation between neural activity and twitches was assessed as follows. First, all twitches of each body part (forelimb, hindlimb, whiskers, tail) were behaviorally scored. For each body part that had more than 20 twitches, perievent histograms of neural activity were constructed (window size: −3 to 3 s; bin size: 10 ms). Next, we determined the mean baseline firing rate from −3 to −0.5 s. Finally, we *Z*-scored the perievent histograms by subtracting the baseline from the raw perievent histograms and dividing this value by the standard deviation of the baseline. A neuron was considered "responsive" to twitches if it showed a clear peak with a *Z*-score of at least 3.5 for at least one body part.

To accurately determine a neuron's preferred somatotopic response (see Figures 3A and S3C), we only analyzed twitches for a given body part that were separated by at least 100 ms from twitches of other body parts. The preferred body part for each neuron was the body part with the largest peak in the *Z*-scored perievent histogram (see Figures 3B and S5F).

Movement Analysis

For each movement type (twitches of different body parts and wake movements), we calculated the average displacement produced by that movement for each pup (see Figure S2D). To ensure subsequent twitches (of the same or different body parts) did not influence the average displacement of a twitch, for this analysis, we used the same subset of twitch triggers used in the somatotopy

Please cite this article in press as: Dooley et al., Movements during sleep reveal the developmental emergence of a cerebellar-dependent internal model in motor thalamus, Current Biology (2021), https://doi.org/10.1016/j.cub.2021.10.014

analysis above (i.e., twitches with inter-twitch-intervals of at least 100 ms). Median average displacement was calculated over all triggered twitches (or wake movements) at each time point. Because the size of the ROI used to assess movements varied across age and body part, median values for each animal were always normalized.

Width at Half- and Three-Quarter-Height

To measure width at half- and three-quarter-height, the displacement and neural data were first smoothed using a 5-bin kernel and then upscaled from 10 ms bins to 1 ms bins using the interp1() function in MATLAB. The data were then normalized so that the baseline was equal to 0 and the peak was set to 1. The width at half-height (in ms) was calculated as the number of bins between 0.5 and 1, and the width at three-quarter-height was calculated as the number of bins between 0.75 and 1.

Statistical Analyses

All statistical tests were performed using MATLAB. Alpha was set at 0.05 for all analyses; when appropriate, the Bonferroni procedure was used to correct for multiple comparisons. Unless otherwise stated, mean data are always reported with their standard error (SE). Normally distributed data were tested for significance using a one-way ANOVA, two-way ANOVA, or t test. Categorical data were tested for significance using a Chi-square test.

Non-normally distributed data were visualized using violin plots, with the red line signifying the median. Two-group data were tested for significance using the Kruskal-Wallis nonparametric test. For individual groups, a Wilcoxon signed-rank test was used. Violin plots were constructed absent outliers, which were determined using the isoutlier() function in MATLAB. This function excludes datapoints that are more than three scaled median-absolute-deviations from the median.

Current Biology, Volume *31*

Supplemental Information

Movements during sleep reveal the developmental emergence of a cerebellar-dependent internal model in motor thalamus

James C. Dooley, Greta Sokoloff, and Mark S. Blumberg

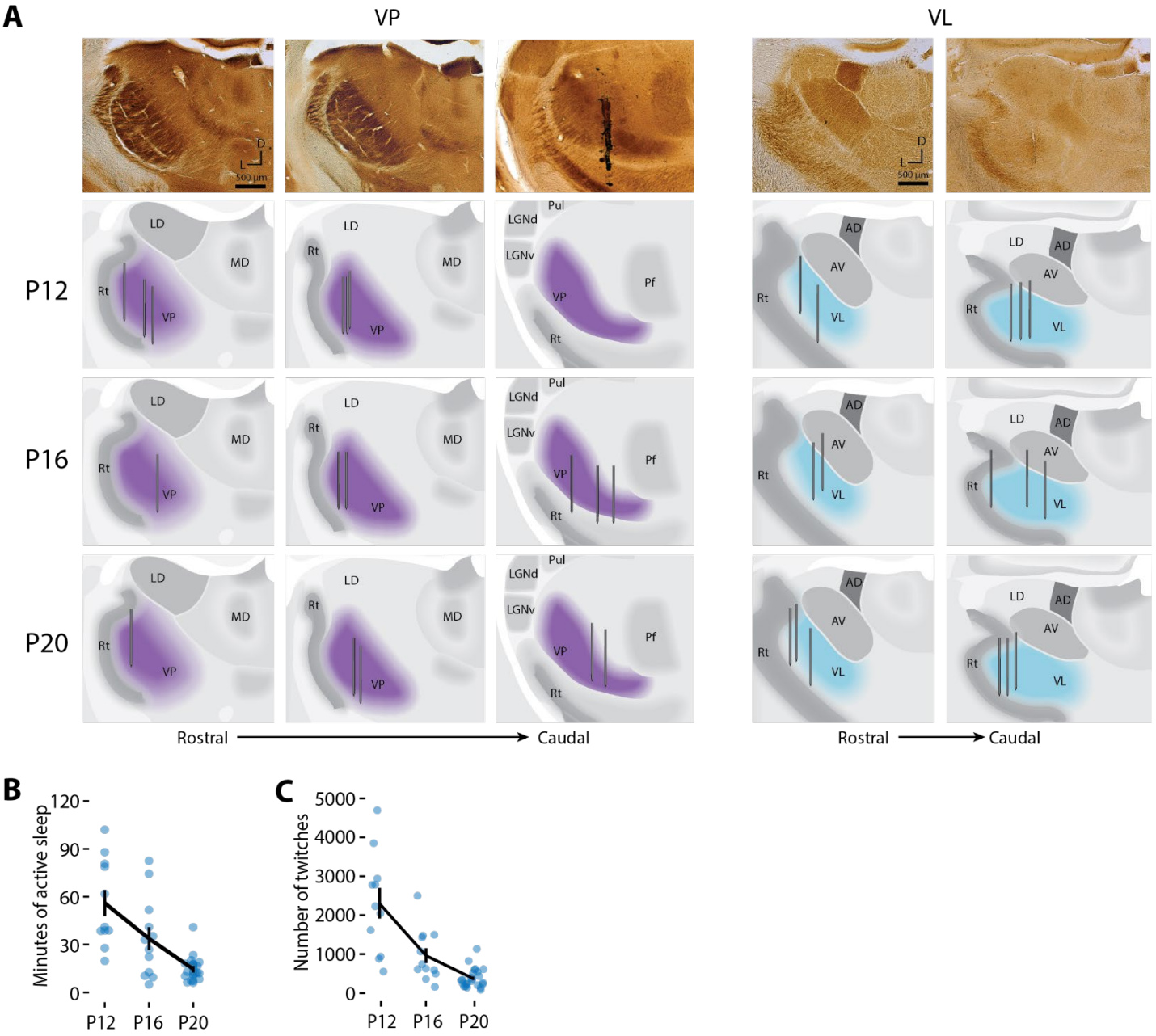

Figure S1. Anatomical and behavioral details, Related to Figure 1.

(A) *Top:* Representative tissue stained for CO showing the rostral to caudal progression of VP (left) and VL (right). VP was differentiated from the surrounding nuclei by its dark appearance in CO-stained tissue. VL was located rostral to VP and appeared lighter than adjacent nuclei (Rt, AV, and VP) in CO-stained tissue. *Bottom:* Location of the recording electrodes in VP (left, purple) and VL (right, cyan) in rats at P12, P16, and P20. CO: Cytochrome oxidase. LD: Lateral dorsal nucleus. MD: Medial dorsal nucleus. Rt: Thalamic reticular nucleus. VP: Ventral posterior nucleus. Pul: Visual pulvinar. LGNd/v: Lateral geniculate nucleus, dorsal and ventral divisions. Pf: Parafascicular nucleus. AD: Anterodorsal nucleus. AV: Anteroventral nucleus. VL: Ventrolateral nucleus.

(B) Mean (± SE) number of minutes of active sleep for each animal across each recording session. Data for individual pups are also shown. The amount of time spent in active sleep decreased significantly across age ($F_{2,44}$ = 18.6, $p < 0.0001$).

(C) Mean (± SE) number of twitches for each animal across each recording session. Data for individual pups are also shown. Twitching decreased significantly across age ($F_{2,44}$ = 26.8, $p < 0.0001$).

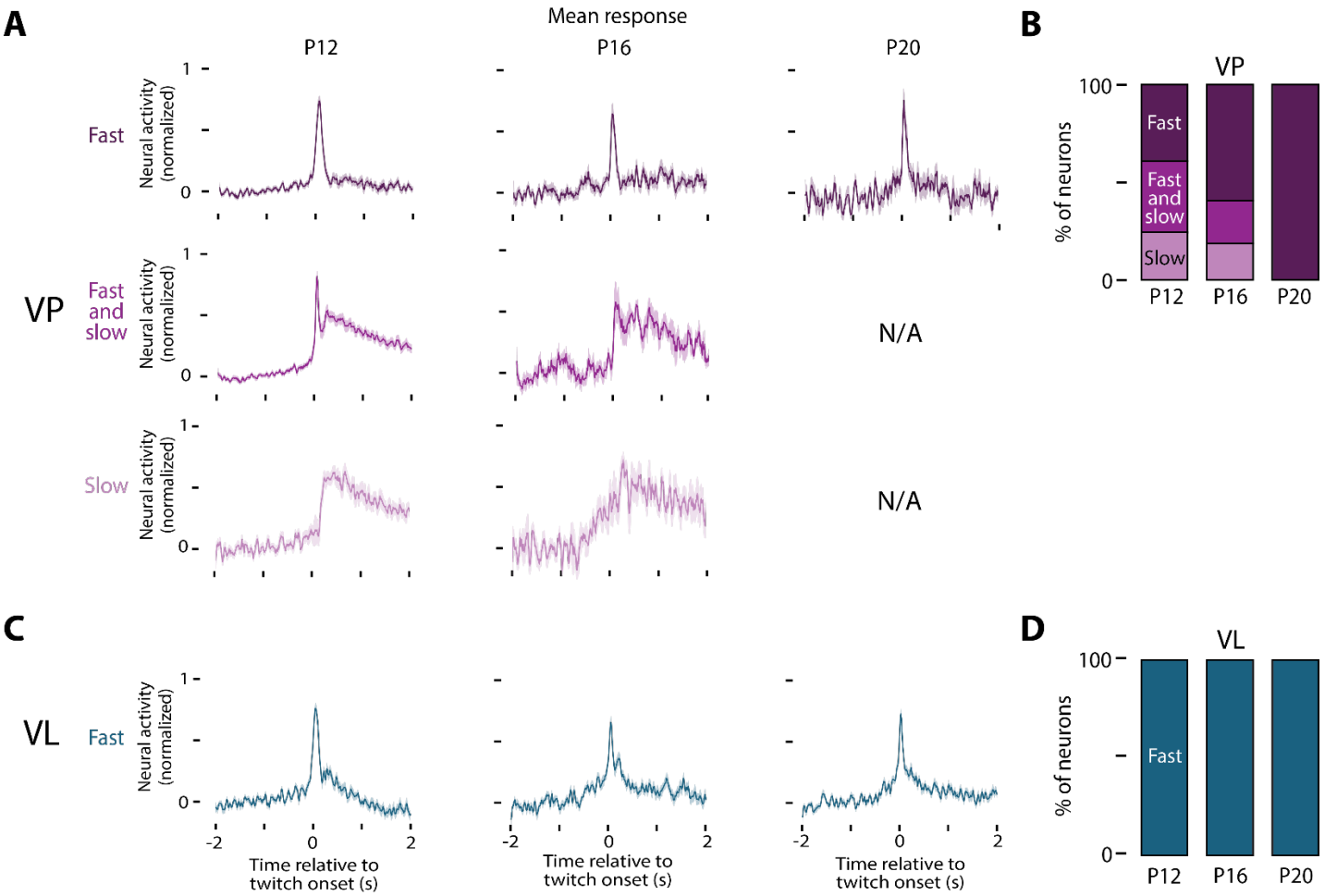

Figure S2. Developmental profiles of fast and slow twitch-responsive thalamic neurons, Related to Figure 2.

(A) Mean (± SE) normalized neural response of VP neurons categorized as fast (top, dark purple), fast and slow (middle, purple), and slow (bottom, light purple) at P12, P16, and P20. N/A indicates an absence of neurons in that category.

(B) Stacked plots showing the percentage of VP neurons categorized as fast, fast and slow, and slow at each age.

(C) Same as in (A), but for VL, for which only fast neurons were observed (dark cyan).

(D) Same as in (B), but for VL.

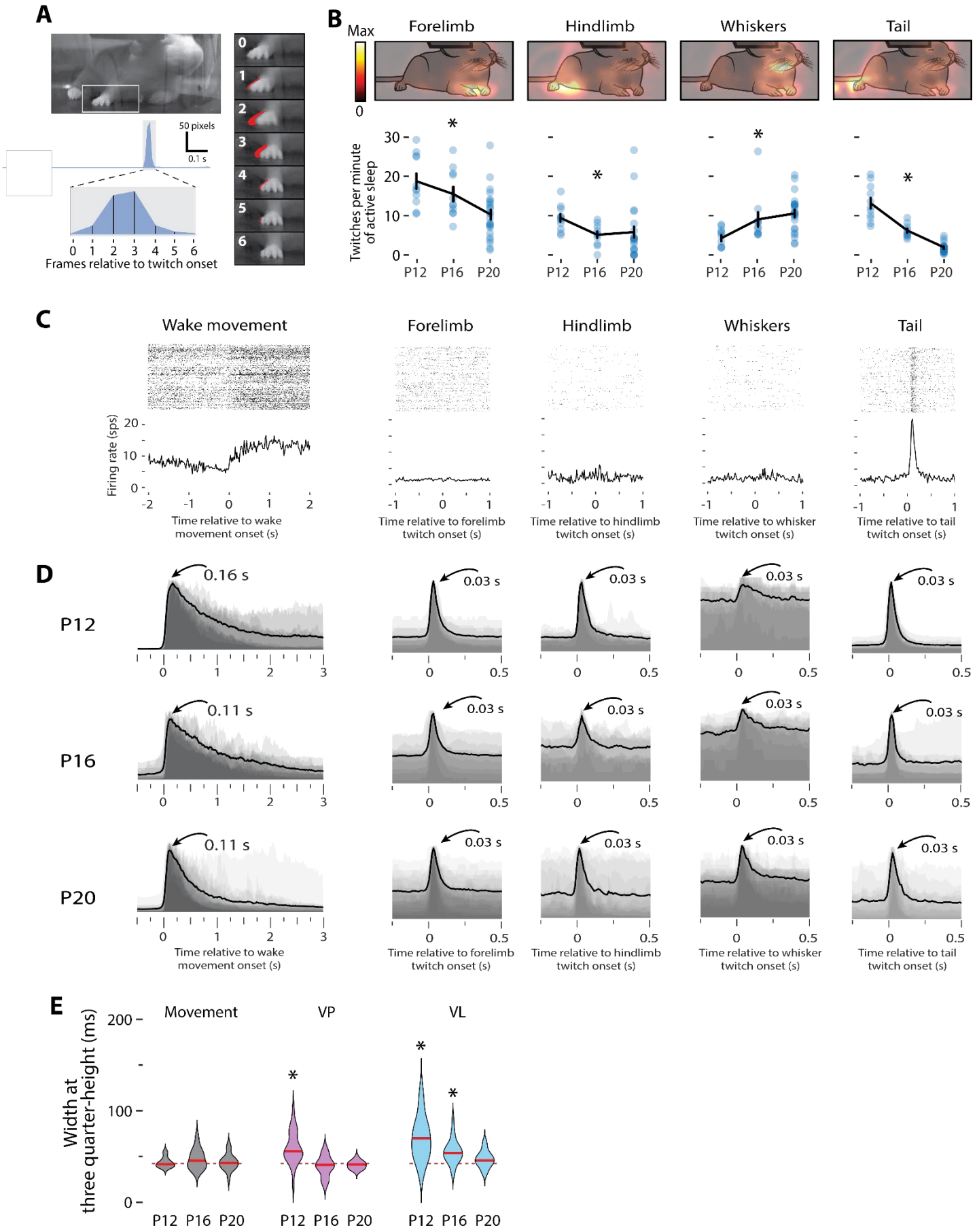

Figure S3. Twitch rates, somatotopy, and kinematics across development, Related to Figure 3.

(A) The image at top-left shows a single frame of a P12 rat just before the onset of a twitch of the forelimb. The area within the white rectangle is shown across seven frames in the panels at right. Starting with the top-most frame (frame 0) and moving down frame by frame, the pixels that change from the previous frame are highlighted in red. The forelimb moves the most in frames 2 and 3 and, by frame 6, the movement has stopped. At left-middle, the output of the twitch-movement analysis for a 1-s interval of active sleep. The region around the twitch (gray box) is expanded below to show the time-course over the seven frames.
(B) *Top*: Drawing of a P20 rat overlaid with a heatmap showing the pixels where movement was most likely to occur in the ten frames after the onset of forelimb, hindlimb, whiskers, and tail twitches. *Bottom*: Mean (± SE) rate of twitches per min of active sleep for twitches of the forelimb, hindlimb, whiskers, and tail across age. Data for individual sessions are also shown. The rate of twitching decreased significantly across age for the forelimbs ($F_{2,44} = 8.01$, $p < 0.005$), hindlimbs ($F_{2,39} = 7.61$, $p < 0.005$), and tail ($F_{2,44} = 62.9$, $p < 0.0001$), but increased for the whiskers ($F_{2,43} = 5.46$, $p < 0.01$).
(C) Perievent histograms for a representative VP neuron at P12 for movements during wake (single panel at left) and twitches during sleep (four panels at right). This neuron responds weakly to wake movements and negligibly to twitches of the forelimb, hindlimb, and whiskers. In contrast, this neuron responses strongly to twitches of the tail, reflecting somatotopic precision.
(D) Mean displacement produced during wake movements, as well as twitches of the forelimb, hindlimb, whiskers, and tail across age. Each shaded gray region denotes the normalized median displacement produced by that movement for an individual pup. The black line is the mean across all pups for that body part and age. For all twitches across all ages, the mean peak displacement occurs 0.03 s (or three frames) after twitch onset.
(E) Violin plots of the width at three-quarters-height for twitch displacement (gray), twitch-responsive VP neurons (magenta), and twitch-responsive VL neurons (cyan) at each age. The solid red line is the median value at each age and the dotted red line is the grand median across all ages. There was no significant age-related change in movement duration ($H_{(2,144)} = 1.54$, $P = 0.46$), but there was a significant effect of age on response duration in VP ($H_{(2,55)} = 22.15$, $P < 0.001$) and VL ($H_{(2,70)} = 17.6$, $P < 0.001$). VP signed rank: P12: $Z_{29} = 4.03$, $P < 0.001$; P16: $Z_{18} = -1.28$, $P = 0.20$; P20: $Z_{10} = -1.27$, $P = 0.20$. VL signed rank: P12: $Z_{27} = 4.19$, $P < 0.001$; P16: $Z_{24} = 3.65$, $P < 0.001$; P20: $Z_{23} = 1.99$, $P = 0.05$. Asterisks indicate that the median value (red line) is significantly different ($P < 0.0167$) from 0.

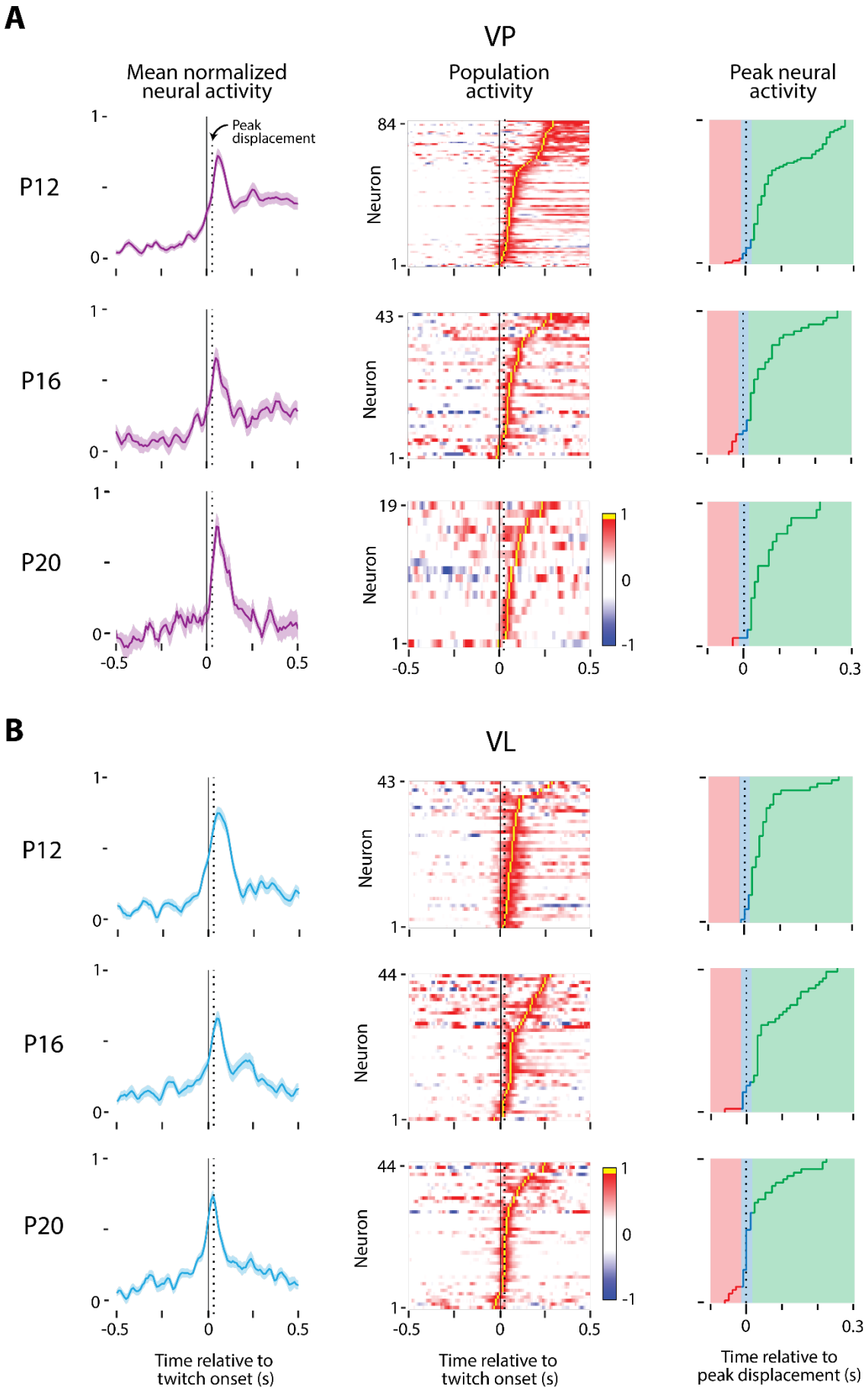

Figure S4. Population-level twitch-related activity in VP and VL, Related to Figure 4.

(A) *Left column*: Mean (± SE) normalized neural activity of twitch-responsive VP neurons across age relative to twitch onset (solid vertical line). Peak twitch displacement, occurring at 0.03 s after twitch onset, is also shown (dotted vertical line). *Middle column*: Heatmap of each twitch-responsive VP neuron's activity relative to a twitch, sorted from bottom by increasing peak time. Each neuron's peak activity (yellow) is represented in the right column. *Right column:* The timing of peak activity for each neuron plotted on top of the categories used to classify neural responses in Figure 4A. Red indicates a neuron that fires before peak displacement, whereas green indicates a neuron that fires after peak displacement. Blue are the neurons that fire within 10 ms of peak displacement.
(B) Same as in (A), but for VL.

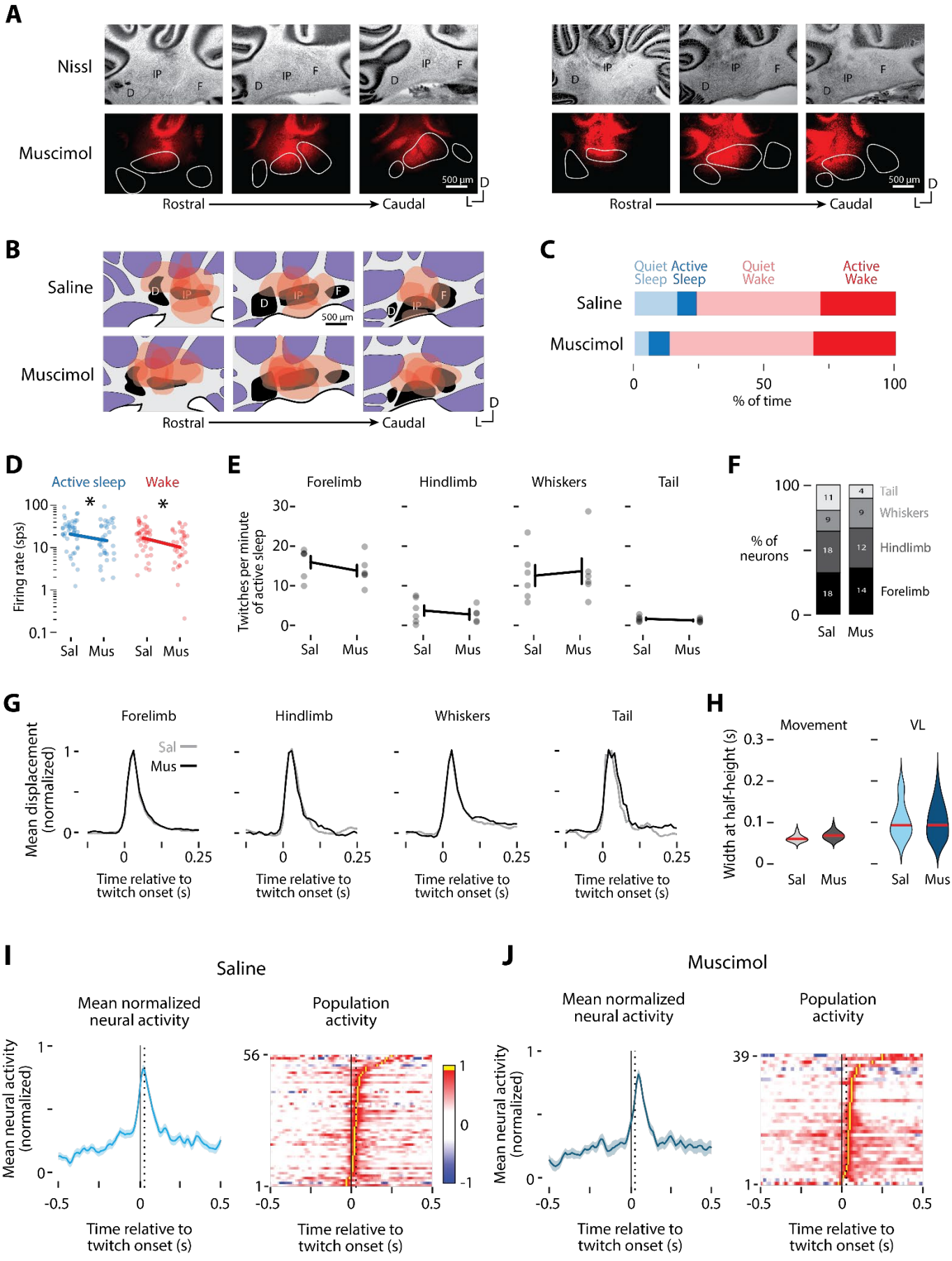

Figure S5. Twitch-related VL activity after injection of muscimol or saline into the DCN at P20, Related to Figure 5.

(A) Diffusion of fluorescent muscimol (bottom row) in three coronal sections through the deep cerebellar nuclei for two pups. The associated Nissl-stained sections are also shown (top row). D: Dentate. IP: Interposed. F: Fastigial.
(B) Drawings of the DCN nuclei across three coronal sections to show the lateral and rostrocaudal diffusion of saline (top) or muscimol (bottom). N=6 per group. Abbreviations as in (A).
(C) Mean percentage of time spent in quiet sleep (light blue), active sleep (dark blue), quiet wake (light red), and active wake (dark red) for pups injected with saline or muscimol.
(D) Mean log-normalized firing rate of VL neurons during active sleep (blue, left) and wake (red, right) following injection of saline (Sal) or muscimol (Mus). Data for individual neurons are also shown. A 2-way ANOVA reveals a significant effect of injection type ($F_{1,152} = 8.42$, $p < 0.005$) but not behavioral state, with muscimol-injected pups showing less neural activity compared to saline animals (denoted by asterisk).
(E) Mean (± SEM) rate of twitches per min of active sleep for twitches of the forelimb, hindlimb, whiskers, and tail across age. Data for individual pups are also shown. None of the differences are statistically significant.
(F) Stacked plots showing the percentage of twitch-responsive VL neurons that respond to twitches of different body part in pups injected with saline (left) or muscimol (right). The number of neurons is also indicated.
(G) Mean normalized movement displacement during twitches of the forelimb, hindlimb, whiskers, and tail in pups injected with saline (gray lines) or muscimol (black lines). The displacement profiles across groups are nearly identical.
(H) *Left*: Mean (± SE) normalized VL activity for saline-injected pups. Peak displacement (0.03 s after twitch onset) is shown as a dotted line. *Right*: Heatmap showing each twitch-responsive neuron's activity relative to a twitch, sorted by peak time. Each neuron's peak activity (yellow) is represented in Figure 5B. The timing of this peak activity relative to peak displacement (dotted line) is used to classify neural responses in Figure 5C.
(I) Same as in (G), but for muscimol-injected pups.
(J) *Left:* Violin plots of the width at half-height for twitch movements for pups injected with saline or muscimol. *Right:* Violin plots of the width at half-height for twitch-responsive VL neurons for pups injected with saline or muscimol. The solid red lines denote median values. Neither of the group differences is significant.